

Improving the Efficiency of Markov Chain Monte Carlo for Analyzing the Orbits of Extrasolar Planets

Eric B. Ford

Astronomy Department, 601 Campbell Hall, University of California at Berkeley, Berkeley, CA 94720-3411, USA

Department of Astrophysical Sciences, Princeton University, Peyton Hall, Princeton, NJ 08544-1001, USA

eford@astron.berkeley.edu

ABSTRACT

Precise radial velocity measurements have led to the discovery of ~ 170 extrasolar planetary systems. Understanding the uncertainties in the orbital solutions will become increasingly important as the discovery space for extrasolar planets shifts to planets with smaller masses and longer orbital periods. The method of Markov chain Monte Carlo (MCMC) provides a rigorous method for quantifying the uncertainties in orbital parameters in a Bayesian framework (Ford 2005a). The main practical challenge for the general application of MCMC is the need to construct Markov chains which quickly converge. The rate of convergence is very sensitive to the choice of the candidate transition probability distribution function (CTPDF). Here we explain one simple method for generating alternative CTPDFs which can significantly speed convergence by one to three orders of magnitude. We have numerically tested dozens of CTPDFs with simulated radial velocity data sets to identify those which perform well for different types of orbits and suggest a set of CTPDFs for general application. Additionally, we introduce other refinements to the MCMC algorithm for radial velocity planets, including an improved treatment of the uncertainties in the radial velocity observations, an algorithm for automatically choosing step sizes, an algorithm for automatically determining reasonable stopping times, and the use of importance sampling for including the dynamical evolution of multiple planet systems. Together, these improvements make it practical to apply MCMC to multiple planet systems. We demonstrate the improvements in efficiency by analyzing a variety of extrasolar planetary systems.

Subject headings: Subject headings: planetary systems – methods: statistical – techniques: radial velocities

1. Introduction

Recent detections of planets around other stars have spurred a wide range of research on planet formation and planetary system evolution. The future of radial velocity planet searches promises to be exciting. Ongoing large surveys including a broad array of nearby main-sequence stars will continue to increase the number of known extrasolar planets. The challenges of accurately determining orbital parameters will become even more important for three reasons. First, continued monitoring with the radial velocity technique will permit the detection of planets with smaller masses. Since the lowest mass planet will always be near the threshold of detection, they will typically have relatively low signal-to-noise ratios and hence relatively large uncertainties in model parameters. Second, the increasing time span of precision observations will permit the discovery of planets with larger orbital periods. Unfortunately, there can be large degeneracies in the orbital parameters for planets with orbital periods comparable to the duration of observations. Finally, the increasing precision and number of radial velocity observations is likely to reveal more multiple planet systems. The large number of model parameters needed to model multiple planet systems can lead to degeneracies and some orbital parameters being poorly constrained. All of these trends imply that it will become increasingly important to understand the uncertainties in orbital elements and other parameters derived from such observations. Thus, we must use the best possible statistical tools to analyze radial velocity data.

1.1. Introduction to Bayesian Inference

To quantitatively analyze the available observational constraints, we employ the techniques of Bayesian inference. The essential equations of Bayesian inference can be easily derived from the basic axioms of probability theory. We start with a joint probability distribution, $p(x, y)$, (x and y may be scalars or vectors of several variables). We then construct a marginalized probability distribution for x by integrating over y , $p(x) = \int p(x, y) dy$. We can then write the joint probability distribution as a product of the marginalized probability distribution and a conditional probability distribution, $p(x, y) = p(x)p(y|x)$. Then, Bayes' theorem could be written as

$$p(y|x) = \frac{p(x, y)}{p(x)} = \frac{p(y)p(x|y)}{\int p(y)p(x|y) dy}. \quad (1)$$

The real insight in Bayes' theorem is to identify x with a set of observational data (\vec{d}) and y with a set of model parameters ($\vec{\theta}$) that are not directly observed. By treating both the observation and the model parameters as random variables, Bayesian inference is able to address statistical questions in a mathematically rigorous fashion. The joint probability, $p(\vec{d}, \vec{\theta})$, can be expressed as the product of the likelihood ($p(\vec{d}|\vec{\theta})$, the probability of the observables given the model parameters), and a prior probability distribution function ($p(\vec{\theta})$) which is based on previous knowledge of the model parameters. Bayes's theorem allows one to compute a posterior probability density function, $p(\vec{\theta}|\vec{d})$,

which incorporates the knowledge gained by the observations \vec{d} . That is

$$\begin{aligned} p(\vec{\theta}|\vec{d}, \mathcal{M}) &= \frac{p(\vec{d}, \vec{\theta}|\mathcal{M})}{p(\vec{d}|\mathcal{M})} = \frac{p(\vec{d}, \vec{\theta}|\mathcal{M})}{\int p(\vec{d}, \vec{\theta}|\mathcal{M})p(\vec{\theta}|\mathcal{M}) d\vec{\theta}} \\ &= \frac{p(\vec{\theta}|\mathcal{M})p(\vec{d}|\vec{\theta}, \mathcal{M})}{\int p(\vec{\theta}|\mathcal{M})p(\vec{d}|\vec{\theta}, \mathcal{M}) d\vec{\theta}}, \end{aligned} \quad (2)$$

where we have now explicitly added the fact that each of the probability distributions is conditioned on the assumption of a certain model, \mathcal{M} , that includes the meaning of the model parameters, $\vec{\theta}$, and their relationship to the observational data, \vec{d} . Table 1 provides a summary of the symbols which appear in multiple sections of this paper.

1.1.1. Advantages of Bayesian Inference

Bayesian inference has several advantages over classical statistical techniques. First, the Bayesian framework provides a rigorous mathematical foundation for making inferences about the model parameters. Since all Bayesian inferences are based on the posterior probability distributions, there is a rigorous basis for quantifying uncertainties in model parameters, unlike frequentist methods which typically result in point estimates. Frequentist methods are often combined with resampling techniques such as bootstrap to estimate uncertainties in model parameters. However, these techniques rely on fictitious observations that the experimenter believes could have been made, while the Bayesian posterior probability distribution depends only on the observations that were actually made (and the prior knowledge of the model parameters). While the posterior probability distribution is often abbreviated as simply the posterior, it is important to remember that it is a true probability distribution for the model parameters, unlike the results of resampling techniques such as bootstrap. Because of these theoretical advantages, Bayesian inference typically produces more accurate estimates of the uncertainty in model parameters, as shown using actual radial velocity observations of extrasolar planet in Ford (2005a, Paper I). For further discussion of alternative techniques see Paper I, §3 & 4.

The Bayesian framework also has several practical advantages. Because inference is based on probability distributions, it is straightforward to incorporate a variety of different types of information and observations. Further, hierarchical Bayesian models can naturally accommodate uncertainties in models as well as in observations. Finally, the Bayesian framework provides a natural basis for making predictions about future observations. These predictions can even be used to improve the efficiency of future experiments or observations (Loredo 2003; Ford 2005b).

The most commonly criticized aspect of Bayesian inference is the necessity of specifying prior probability distributions for the model parameters. In many cases, the observational data provides such a strong constraint on the model parameters that the effect of the prior is negligible. However, in cases where the observations provide only very limited constraints, the posterior distribution can

be significantly influenced by the choice of prior. A complete Bayesian analysis should include checking the sensitivity of any conclusions to the choice of prior. It should be noted that this criticism is not unique to Bayesian inference. Similar assumptions are being made implicitly in frequentist analyses, as the choice of model parameters can also significantly influence the results. For a striking example of practical differences for orbit determination of binary stars, see Pourbaix (2002). Indeed, the necessity to explicitly state what priors are being chosen can be viewed as a strength of the Bayesian method.

Given all the advantages of Bayesian inference, one might wonder why it is not the standard practice for data analysis in the physical sciences. Unfortunately, the lower integral in Eqn. 2 can be extremely difficult to compute, particularly when $\vec{\theta}$ has a large number of dimensions. The computational burden has long limited Bayesian methods to a small number of relatively simple problems. Modern computers permit the application of Bayesian inference to an growing number of increasingly complex problem. Even today, the brute force evaluation of the integrals is impractical for many real world problems. Therefore, it is necessary to develop efficient algorithms for evaluating the necessary integrals. The method of Markov chain Monte Carlo is quite general and it has become an increasingly common tool for performing the necessary Bayesian integrals in recent years (e.g., Paper I and reference therein).

1.2. Introduction to Markov chain Monte Carlo

Paper I introduced Bayesian analysis for constraining the orbital parameters of extrasolar planets with radial velocity observations and presented an algorithm to perform the necessary integrations based on Markov chain Monte Carlo (MCMC) simulation. This algorithm can accurately characterize the posterior probability distribution function for orbital parameters based on radial velocity observations.

Paper I described how to construct a Markov chain (i.e. sequence) of states (i.e. sets of parameter values, $\vec{\theta}_i$) which are sampled from the posterior probability function. Such a chain can be calculated by specifying an initial set of parameter values, $\vec{\theta}_0$, and a transition probability, $p(\vec{\theta}_{i+1}|\vec{\theta}_i, \mathcal{M})$. To guarantee that the Markov chain will converge to the posterior probability distribution, the Markov chain must be aperiodic, irreducible (i.e., it must be possible for the chain to reach every state with non-zero probability from any other state with non-zero probability), and reversible, that is,

$$p(\vec{\theta}|\vec{d}, \mathcal{M})p(\vec{\theta}|\vec{\theta}', \mathcal{M}) = p(\vec{\theta}'|\vec{d}, \mathcal{M})p(\vec{\theta}'|\vec{\theta}, \mathcal{M}). \quad (3)$$

It is possible to construct a reversible transition probability, $p(\vec{\theta}'|\vec{\theta}, \mathcal{M})$, from a non-reversible candidate transition probability distribution function (CTPDF), $q(\vec{\theta}'|\vec{\theta}, \mathcal{M})$, using the Metropolis-Hastings (MH) algorithm. The MH algorithm involves the generation of a trial state ($\vec{\theta}'$) according to the CTPDF, $q(\vec{\theta}'|\vec{\theta}, \mathcal{M})$, and randomly accepting the trial as the next state or rejecting the trial

state in favor of the current state. The MH algorithm specifies an acceptance probability

$$\alpha(\vec{\theta}'|\vec{\theta}, \mathcal{M}) = \min \left\{ \frac{p(\vec{\theta}'|\vec{d}, \mathcal{M})q(\vec{\theta}|\vec{\theta}', \mathcal{M})}{p(\vec{\theta}|\vec{d}, \mathcal{M})q(\vec{\theta}'|\vec{\theta}, \mathcal{M})}, 1 \right\} \quad (4)$$

$$= \min \left\{ \frac{p(\vec{d}|\vec{\theta}', \mathcal{M})q(\vec{\theta}|\vec{\theta}', \mathcal{M})}{p(\vec{d}|\vec{\theta}, \mathcal{M})q(\vec{\theta}'|\vec{\theta}, \mathcal{M})}, 1 \right\}. \quad (5)$$

When using this acceptance probability, the transition probability

$$p(\vec{\theta}'|\vec{\theta}, \mathcal{M}) = q(\vec{\theta}'|\vec{\theta}, \mathcal{M})\alpha(\vec{\theta}'|\vec{\theta}, \mathcal{M}) \quad (6)$$

is guaranteed to be reversible and irreducible, provided only that $q(\vec{\theta}'|\vec{\theta}, \mathcal{M})$ allows transitions to all $\vec{\theta}'$ for which $p(\vec{\theta}'|\vec{d}, \mathcal{M})$ is non-zero. Note that the MH algorithm does not require that the normalization of $p(\vec{\theta}'|\vec{d}, \mathcal{M})$ be known.

While the above algorithm guarantees that the Markov chain will converge to $p(\vec{\theta}'|\vec{d}, \mathcal{M})$, it does not specify when the chain will achieve convergence. The choice of $q(\vec{\theta}'|\vec{\theta}, \mathcal{M})$ can have a dramatic effect on the rate of convergence of the Markov chain. Poor choices can lead to extremely inefficient sampling and hence slow convergence. The most efficient choice for $q(\vec{\theta}'|\vec{\theta}, \mathcal{M})$ would be $p(\vec{\theta}'|\vec{d}, \mathcal{M})$, the posterior probability distribution itself. However, this is rarely possible, since the whole purpose of the Markov chain is to calculate the posterior distribution.

Paper I presented a practical algorithm based on the Metropolis-Hastings algorithm, varying a subset of parameters at each step, and a Gaussian CTPDF, $q(\vec{\theta}'|\vec{\theta}, \mathcal{M})$ centered on $\vec{\theta}$ with a covariance matrix $I\vec{\beta}$, where I is the identity matrix and $\vec{\beta}$ is a vector of scale parameters, β_ν . Throughout this paper, we use the index ν to distinguish the model parameters. The Gibbs sampler specifies that only a subset of $\vec{\theta}$ is altered at each step of the Markov chain. While there are several variations, we choose which parameters are to be altered in the next trial state according to randomly generated permutations of the model parameters. At each step one function of the model parameters ($u_\mu(\vec{\theta})$) is chosen to be updated using,

$$q(u_\mu(\vec{\theta}')|u_\mu(\vec{\theta}), \mathcal{M}) = \frac{1}{\sqrt{2\pi\beta_\mu^2}} \exp \left[-\frac{[u_\mu(\vec{\theta}') - u_\mu(\vec{\theta})]^2}{2\beta_\mu^2} \right] \quad (7)$$

for valid $\vec{\theta}'$ (i.e., if the model dictates that $\vec{\theta}'_\nu$ be positive definite, then trial states with negative $\vec{\theta}'_\nu$ are rejected). We use the index μ to distinguish the different types of steps, and the index i to indicate the n -th step of the Markov chain. Each β_μ is a parameter which controls the scale for the steps based on the quantity indicated by μ . In Paper I, we used $\vec{u}(\vec{\theta}) = \vec{\theta}$, i.e., we only took steps in the model parameters. In §4 of this paper, we will present several alternative CTPDFs that can significantly improve the computational efficiency of the MCMC algorithm by reducing the number of steps required before a Markov chain can be used for inference.

1.3. Summary of Previous Results

The techniques of Bayesian inference and Markov chain Monte Carlo have previously been applied to analyzing the radial velocity observations of several extrasolar planetary systems. Originally, Paper I presented a complete algorithm for calculating the posterior probability distributions for orbital parameters based on radial velocity observations. Paper I demonstrated several shortcomings of the conventional estimates of parameter uncertainties based on bootstrap-type resampling. It found that Bayesian analyses, were particularly important for planets where the orbital period is comparable to the duration of observations. Driscoll (2006) is performing a systematic study to compare uncertainty estimates made with bootstrap-style resampling and uncertainty estimates made with MCMC. Gregory (2005a) used Bayesian inference and MCMC to reanalyze the observations of one particular system (HD 73526), and found two alternative orbital solutions, one of which had a larger posterior probability than the originally published orbital solution. This demonstrated another shortcoming of frequentist methods that are based on only the maximum likelihood solution, rather than the posterior probability distribution. Ford, Lystad & Rasio (2005) reanalyzed the observations of the three planets orbiting ν Andromedae to derive improved constraints on the orbital parameters and perform a dynamical analysis (Ford et al. 2005). Gregory (2005b) used an improved algorithm to analyze another system (HD 208487) and claim that the present data show a $\sim 95\%$ probability for a second planet.

1.4. Motivation for this work

Each of the above studies using MCMC has demonstrated advantages of Bayesian inference for analyzing radial velocity observations of extrasolar planets. However, significant obstacles remain. For several of the systems analyzed in Paper I, the model parameters were highly correlated and caused the Markov chains to converge slowly. Convergence was particularly problematic for multiple planet systems, so Paper I included an analysis of only one multiple planet system (GJ 876). While we had attempted to include other multiple planet systems, slow convergence rates and computational limitations prevented us from being sufficiently confident that the other Markov chains had converged to include them in the final paper. Gregory (2005a) took the more risky approach of basing inferences on Markov chains which showed obvious signs of non-convergence, but argued that the main conclusions were robust. These studies illustrate the importance of improving the computational efficiency of MCMC algorithms for analyzing radial velocity data.

Since Paper I, we have dramatically improved the computational efficiency of our MCMC algorithm by introducing alternative CTPDFs. Our improved CTPDFs allow for the very rapid analysis of the typical single planet systems, as well as the practical application of Bayesian inference and MCMC to multiple planet systems. For example, incorporating just a few of these optimizations permitted the dynamical analysis of the ν Andromedae system (Ford et al. 2005).

1.5. Outline

In this paper we describe several refinements to the algorithms presented in Paper I. In §2 we present our physical model of the planetary system and observations. We include modifications to the model that allow the MCMC technique to be applied to systems with a significant amount of stellar “jitter” and/or additional unknown planetary companions. We also present a method for testing the sensitivity of posterior distribution functions to the assumption that the observational uncertainties are normally distributed. In §3 we provide precise descriptions of a few important technical issues, including choosing priors, choosing step sizes, testing for non-convergence, and deciding when to stop calculating Markov chains. In §4 we describe modifications to the original MCMC algorithm presented in Paper I. In particular, we present several alternative choices for the CTPDF, $q(\vec{\theta}'|\vec{\theta})$, and demonstrate the improved efficiency by applying the new sampling algorithms to several different types of simulated planetary systems. Of particular interest, we make practical suggestions for the choices of CTPDFs in §4.13. In §5, we discuss the application to multiple planet systems. In §6, we demonstrate our improved algorithms on a few examples of actual planetary systems. In §7, we summarize our conclusions and discuss areas for future research.

2. Model

Here we present our model for the planetary system and the observations, including several sources of noise.

2.1. Model of Planetary System

Since we are interested in planetary mass bodies, the dynamics is described by the gravitational interactions of several point mass bodies. Specifying the mass and six phase space coordinates of each body at a specified time would provide a complete description of the system. Shifting into the center of mass frame can eliminate one set of phase space coordinates. In practice, it is convenient to choose the osculating Keplerian orbital elements (orbital period, P , orbital eccentricity, e , inclination relative to the plane of the sky, i , argument of periastron measured from the plane of the sky, ω , longitude of ascending node, Ω , and mean anomaly, M) in Jacobi coordinates. The observed stellar velocity is the sum of the line of sight velocity of the center-of-mass and the projection of the reflex velocity due to any planetary companions onto the line of sight. For multiple planet systems, it can be important to use complete n-body simulations to model the planetary motions accurately (e.g., GJ876; Laughlin et al. 2005; Rivera et al. 2005). However, in many cases, the mutual planetary perturbations are negligible on time scales comparable to the duration of observations. In such cases, the radial velocity perturbations due to a multiple planet system can be modeled as the linear superposition of multiple unperturbed Keplerian orbits.

For a planet on an unperturbed Keplerian orbit, the mean anomaly is the only one of the Keplerian orbital elements that changes with time. The perturbation to the stellar radial velocity ($\Delta v_{*,p}$) due to a planet on a Keplerian orbit is given by

$$\Delta v_{*,p}(t) = K_p [\cos(\omega_p + T_p) + e_p \cos(\omega_p)] \quad (8)$$

where p labels the planet, K is the velocity semi-amplitude and T is the true anomaly, which implicitly depends on time. The true anomaly (T) is related to the eccentric anomaly (E) via the relation

$$\tan\left(\frac{T}{2}\right) = \sqrt{\frac{1+e}{1-e}} \tan\left(\frac{E}{2}\right). \quad (9)$$

The eccentric anomaly is related to the mean anomaly (M) via Kepler’s equation

$$E(t) - e \sin(E(t)) = M(t) - M_o = \frac{2\pi}{P}(t - \tau) \quad (10)$$

where M_o is a constant, the orbital phase at $t = \tau$. The velocity semi-amplitude can be related to the planet mass, m , by

$$K = \frac{m \sin i}{M_*} \left(\frac{2\pi GM_*}{P}\right)^{1/3} (1 - e^2)^{-1/2} \left(1 + \frac{m}{M_*}\right)^{-2/3} \quad (11)$$

where M_* is the stellar mass and G is the gravitational constant.

Unfortunately, radial velocity observations alone do not measure the orbital inclination relative to the plane of the sky (i), the longitude of ascending node (Ω) or the planet mass. The minimum mass ratio, $m_{\min}/M_* = m \sin i/M_*$ can be determined from Eqn. 11 iteratively. When only radial velocity observations are used to constrain the orbital elements, we simply exclude i and Ω from the set of model parameters for planet p , $\vec{\vartheta}_p = (\log P_p, \log K_p, e_p, \omega_p, M_{o,p})$. However, when additional constraints are available (e.g., astrometric or dynamical), these can be constrained and should be included in $\vec{\vartheta}_p = (\log P_p, \log K_p, e_p, \omega_p, M_{o,p}, \cos i_p, \Omega_p)$.

2.2. Model of Observations

In radial velocity surveys, the velocity of the central star is precisely monitored for periodic variations which could be caused by orbiting companions. Each individual observation can be reduced to an estimate of the observational uncertainty ($\sigma_{k,\text{obs}}$) and a measurement of the star’s radial velocity ($v_{*,\text{obs}}(t_k, j_k)$), where t_k is the time of the k th observation and j_k specifies the observatory and spectrometer used for the k th observation. Because each radial velocity measurement is based on calculating the centroid of thousands of spectra lines and averaged over hundreds of sections of the spectrum, the observational uncertainties of most current echelle based radial velocity surveys can be accurately estimated and are nearly Gaussian (Butler et al. 1996). If the observational data

(\vec{d}) were generated by the model specified by $\vec{\theta}$, then the probability of drawing the observed values is

$$p(\vec{d}|\vec{\theta}, \mathcal{M}) = \prod_k \frac{1}{\sqrt{2\pi}\sigma_k} \exp \left[-\frac{(d_{k,\theta} - d_k)^2}{2\sigma_k^2} \right], \quad (12)$$

assuming that the errors in individual observations are normally distributed and uncorrelated. Here $d_k \equiv v_{*,\text{obs}}(t_k, j_k)$ is the observed velocity at time t_k as measured by observatory and spectrometer j_k , $d_{k,\theta} = v_{*,\vec{\theta}}(t_k, j_k)$ is predicted velocity according to the model parameters $\vec{\theta}$, and σ_k is the uncertainty in the k th observation. If there are no sources of noise other than the measurement uncertainties, $\sigma_{k,\text{obs}}$, then we can use Eqn. 12, setting $\sigma_k = \sigma_{k,\text{obs}}$. Since the observational uncertainties are all assumed to be Gaussian and uncorrelated, it is convenient to use the χ^2 statistic,

$$\chi^2 = \sum_k \left[v_{*,\vec{\theta}}(t_k, j_k) - v_{*,\text{obs}}(t_k, j_k) \right]^2 / \sigma_k^2. \quad (13)$$

If the planets are on non-interacting Keplerian orbits, then

$$v_{*,\vec{\theta}}(t, j) = C_j + \sum_p \Delta v_{*,p}(t), \quad (14)$$

where C_j is the velocity constant for the observatory/spectrograph labeled by subscript j , and $\Delta v_{*,p}(t)$ is given by Eqn. 8. While there is a single mean line of sight velocity of the center of motion, it is important to use separate constants, C_j for each observatory/spectrograph pair due to potential differences in the calibrations. In the next section we discuss observational uncertainties and present reasons why the values of σ_k may depend on the model parameters.

2.3. Observational Uncertainties and Other Sources of Noise

In Paper I, we analyzed chromospherically inactive stars and assumed that the uncertainties in individual observations were well estimated. Therefore, we set $\sigma_k = \sigma_{k,\text{obs}}$. However, for many stars the distribution of χ^2 calculated with the actual data and models drawn from the posterior distribution was larger than would be expected if the model were correct. Even if the observational uncertainties are perfectly estimated, there could be additional causes of radial velocity variations that are not included in the model. We explore the two most important causes of “jitter” below. Then, we modify the methods described above to allow for an additional source of observational uncertainty of unknown magnitude.

2.3.1. Stellar Jitter

For many stars the small chromospheric emission suggests that the observational uncertainties are dominated by photon noise. Indeed, the quoted uncertainties in the radial velocity observations have been demonstrated to be quite accurate for some chromospherically inactive stars with no

signs of planets (Wright 2005). However, for other stars, the radial velocity observations can be contaminated by stellar “jitter” due to stellar phenomena such as stellar oscillations, convective motions, starspots.

The true distribution for the stellar jitter is unknown. One of the primary sources of stellar jitter is believed to be stellar p-mode oscillations. Indeed, such oscillations have been detected for a few stars by taking a rapid series of high precision radial velocity observations (e.g., Kjeldsen et al. 2003; Butler et al. 2004). We treat the jitter as an additional source of Gaussian noise with variance σ_{jitter}^2 . This is an excellent approximation for two reasons. First, the stellar jitter will be convolved with the Gaussian observational uncertainty. Second, stellar oscillations would result in a periodic signal of finite amplitude, so the jitter distribution would be symmetric and have smaller tails than a Gaussian distribution with the same variance. Thus, we expect that approximating the jitter as an additional source of Gaussian noise will be highly accurate. To test this assumption, we have analyzed a large number of observations of the star τ Ceti taken by the California & Carnegie planet search (Fischer, private communication). We find that the distribution of the velocities for τ Ceti is consistent with a normal distribution, and conclude that the above treatment of stellar jitter is adequate for the purposes of this paper.

2.3.2. Additional Unseen Companions

Another potential source for excess scatter in the residuals is the presence of additional undetected companions. When the number of observations is small ($\lesssim 50$), it can be possible to detect a significant increase in the scatter, even if it is not possible to identify an orbital solution which significantly reduces χ^2 (Cumming et al. 2003). Since the amplitude, eccentricity, and argument of pericenter of any undetected companions is unknown, the exact distribution of these perturbations is unknown. While it is theoretically possible to calculate the distribution of the perturbations based on the prior distributions for $\log K$, e , and ω , we note that this distribution is symmetric and has tails that are less than that of a normal distribution with the same variance. Additionally, the distribution of the perturbations will be convolved with the Gaussian observational uncertainties. Therefore, the distribution of the perturbations can be conveniently approximated as normal with zero mean and variance σ_{unseen}^2 . We can easily incorporate the perturbations due to both stellar “jitter” and unseen companions by using Eqn. 12 and setting $\sigma_k^2 = \sigma_{k,\text{obs}}^2 + \sigma_+^2$, where $\sigma_+^2 = \sigma_{\text{jitter}}^2 + \sigma_{\text{unseen}}^2$.

2.3.3. Correlated Residuals

The above treatment of stellar jitter and undetected companions assumes that the velocity perturbations due to these effects are uncorrelated in time. If the stellar jitter is due to convection or stellar oscillations, then we expect significant correlation over minute time scales, but not days.

On the other hand, if star spots introduce significant stellar jitter, then there could be correlations on time scales comparable to the rotation period (ones to tens of days). If an undetected planet has an orbital period of just a few days, then the residuals for observations on consecutive nights could have a significant correlation, but observations made during consecutive months would typically have a negligible correlation. In this case the posterior distribution for the planets detected with significantly longer periods will generally be near the actual parameters but with an increased dispersion due to the “noise” from the undetected planet. However, if an undetected companion has an orbital period longer than the typical spacing of observations, then the residuals at consecutive observation times will be correlated, possibly resulting in a systematic effect on the posterior distribution for the orbital parameters of the detected planets. The magnitude of the velocity perturbations should be small (since the planet is presumed to be undetected), so in many cases the effect on the orbital parameters for the detected planets is still expected to be small. However, in some cases the perturbations of an undetected planet can be largely compensated for by a change in the orbital parameters of the detected planets (e.g., the inner planet in a 2:1 mean motion resonance can have an effect similar to an eccentricity for the outer planet). In such cases, the resulting posterior distribution may be biased by the unseen companion. Simply increasing the effective observational uncertainty does not account for the correlation between observations due to the unknown companion. This potential bias could be removed by including the possibility of additional unknown companions in the model and marginalizing over their orbital parameters. Unfortunately, this would be computationally quite demanding, since the allowed orbital parameters for the unknown companion will likely span the entire allowed parameter space. Nevertheless, if the radial velocity signature of a distant companion is even marginally detected, then the distant companion should be properly incorporated into the model, even if the observations provide only limited constraints on the orbital parameters. This provides yet another motivation to improve the efficiency of MCMC algorithms for analyzing radial velocity data.

2.4. Models with Noise of Unknown Magnitude

The radial velocity perturbations due to stellar jitter and undetected planets can be incorporated into our models by assuming that the jitter causes a perturbation to the radial velocity at each observation. If we assume that the perturbations due to “jitter” are uncorrelated and drawn from a normal distribution with zero mean and variance σ_+^2 , then the expectation of $v_{*,\vec{\theta}}(t_k, j_k)$ is unchanged, but the distribution of the residuals, $v_{*,\text{obs}}(t_k, j_k) - v_{*,\vec{\theta}}(t_k, j_k)$, is normal with a variance equal to $\sigma_{k,\text{obs}}^2 + \sigma_+^2$. The probability of the observations (\vec{d}) given the model ($\vec{\theta}$) is given by Eqn. 12 by setting $\sigma_k^2 = \sigma_{k,\text{obs}}^2 + \sigma_+^2$ (Gregory 2005a). If the value of each σ_k were known *a priori*, the terms outside the exponential are constant from model to model, they cancel when considering the ratio $p(\vec{d}|\vec{\theta}', \mathcal{M})/p(\vec{d}|\vec{\theta}, \mathcal{M})$ for calculating the acceptance probability with in Eqn. 5. When the value of σ_+ is not known *a priori*, it must be estimated along with the other parameters in $\vec{\theta}$. The terms outside the exponential of Eqn. 12 are no longer the same for all models. Therefore, when

a candidate transition step varies σ_+ , the acceptance rate will depend on the values of σ_+ for the two models, both due to the effect on $\chi^2(\vec{\theta}') - \chi^2(\vec{\theta})$ and due to the ratio

$$\frac{\prod_k \left(\sigma_{k,\text{obs}}^2 + \sigma_+^2 \right)^{1/2}}{\prod_k \left(\sigma_{k,\text{obs}}^2 + \sigma_+'^2 \right)^{1/2}}. \quad (15)$$

This latter factor penalizes models for which σ_+ would result in a larger dispersion of velocity residuals than are contained in the actual data. For observational data which requires a significant noise component, a small value of σ_+ is penalized by the effect on χ^2 .

Since σ_+ is a scale parameter, it would be natural to use the non-informative prior $p(\sigma_+) \sim \sigma_+^{-2}$. However, a prior for σ_+ that is flat on $\log \sigma_+$ is improper, i.e., the prior probability distribution function is not normalizable. If a significant value of σ_+ is required to match the observational data, then the posterior distribution will be normalizable. If the observational data requires that any noise source be small compared to the observational uncertainties, $\sigma_{k,\text{obs}}$, then the posterior distribution is likely to be non-normalizable, but the value of the parameter σ_+ will not make a significant difference in the model predictions. In such a case, new Markov chains could be calculated with σ_+ held fixed at $\sigma_+ = 0$ to provide a properly normalized posterior distribution. We can avoid this complication by using a normalized prior for σ_+ . For example, we could impose sharp lower and upper limits, $-5 \leq \log \sigma_+ \leq 7$. An alternative is to use the Jefferies prior,

$$p(\sigma_+) = (\sigma_{+,o} + \sigma)^{-1} \left[\ln \left(\frac{\sigma_{+,o}}{(\sigma_{+,o} + \sigma)} \right) \right]^{-1}, \quad (16)$$

which is also properly normalized (Gregory 2005a).

Finally, we note that allowing the model to include a noise source with unknown magnitude can have practical benefits when a Markov chain is started far from the best-fit solutions. If χ^2 is calculated assuming only observational uncertainties, then the χ^2 surface is often very “rough” with many local minima and maxima scattered throughout parameter space. However, when an unknown noise source is included in the model and the current state has a large χ^2 , then the Markov chain will increase σ_+ so that χ^2 is comparable to the number of degrees of freedom (number of observations minus number of free parameters). This will result in smoothing out the χ^2 surface (at constant σ_+) and allow the Markov chain to explore the parameter space more quickly. The Markov chain will begin to decrease the values of σ_+ as the Markov chain settles in near the best-fit parameters. This behavior is similar to simulated annealing, but does not require choosing a cooling schedule in advance. Thus, including a noise source of unknown magnitude can have the additional benefit of reducing the number of steps required for a Markov chain to go from an initial state to the region of parameter space near the best-fit solution. This is particularly useful when the Markov chains will be tested for non-convergence using tests which require that the Markov chains be started from widely dispersed initial conditions, such as the Gelman-Rubin test (see §3.3).

2.4.1. Non-Gaussianities & Robust Statistics

In the above treatment we have assumed that the distribution for the unknown radial velocity perturbations is normal. Since the actual distribution of “stellar jitter” (or other poorly understood noise sources) is unknown, one might worry about the robustness of conclusions based on the assumption of normality. Here we introduce a method for testing the sensitivity of conclusions to this assumption. We replace the normal distribution, $N(0, \sigma_k)$ for each of the velocity residuals with a Student’s t distribution with ν degrees of freedom ($t_\nu(0, \sigma_k)$). In the limit that $\nu \rightarrow \infty$, the distribution $t_\nu(0, \sigma_k)$ approaches the normal distribution, $N(0, \sigma_k)$. For $\nu \leq 2$ the tails of the t_ν distribution are so large that the variance is undefined.

To implement this alternative assumption about the distribution of errors, we replace Eqn. 12 with

$$p_\nu(\vec{d}|\vec{\theta}) = \prod_k \frac{\Gamma((\nu+1)/2)}{\Gamma(\nu/2)\sqrt{\nu\pi}\sigma_k} \left[1 + \frac{1}{\nu} \left(\frac{v_{*,\vec{\theta}} - v_{*,\text{obs}}}{\sigma_k} \right)^2 \right]^{-(\nu+1)/2}, \quad (17)$$

where both $v_{*,\vec{\theta}}$ and $v_{*,\text{obs}}$ are functions of t_k and j_k . It is then possible to compute multiple posterior distributions parameterized by ν . In principle, ν could be treated as an unknown hierarchical model parameter and directly estimated from the observational data with the standard Bayesian techniques. In most cases, the posterior probability (marginalized over all model parameters other than ν) reveals a lower bound on ν , $\nu_{\text{min}} > 2$, since $\lim_{\nu \rightarrow 2} \text{var}(t_\nu(0, \sigma_k)) = \infty$. In practice, a very large number of observations is required to characterize the wings of the probability distribution for the observational data (Gelman et al. 2003). Therefore, in typical cases, it is not possible to place an upper bound on ν , since $\lim_{\nu \rightarrow \infty} t_\nu(0, \sigma_k) \sim N(0, \sigma_k)$, corresponding to the case where observational uncertainties are due to photon noise alone. Unless there is a good reason for believing that the velocity residuals follow a t -distribution with a particular value of ν , the posterior distributions calculated using a t_ν distribution ($p_\nu(\vec{\theta}|\vec{d})$), should not be regarded as a robust estimate of the posterior distribution. Rather, we recommend that researchers analyze posterior distributions with multiple values of ν to determine the sensitivity of inferences made to the assumed distribution for the velocity residuals (e.g., as in Ford et al. 2005). If there are significant differences between inferences based on $p_\infty(\vec{\theta}|\vec{d})$ and $p_{\nu_{\text{min}}}(\vec{\theta}|\vec{d})$, then one should realize that the inference depends on the assumed distribution for the velocity residuals. If the same inferences could be made from either $p_\infty(\vec{\theta}|\vec{d})$ or $p_{\nu_{\text{min}}}(\vec{\theta}|\vec{d})$, then the inferences can be considered robust to the assumptions that observational uncertainties and other sources of noise are normally distributed.

3. Technical Issues Relating to MCMC

We have summarized the essential elements of the MCMC algorithm in §1.2 and our models for analyzing radial velocity observations of extrasolar planetary systems in §2. Here we discuss a few technical issues related to the practical implementation of our MCMC algorithm.

3.1. Choice of Priors

We choose a uniform prior in each of the parameters in $\vec{\theta} = (\vec{v}, \vec{C}, \log \sigma_+)$. Remember that $\vec{v}_p = (\log P_p, \log K_p, e_p, \omega_p, M_{o,p})$ if radial velocity observations are the sole constraint or $\vec{v}_p = (\log P_p, \log K_p, e_p, \omega_p, M_{o,p}, \cos i_p, \Omega_p)$ if additional constraints are available, where P is the orbital period, K is the velocity semi-amplitude, e is the orbital eccentricity, ω is the argument of periastron, and M_o is the mean anomaly at the chosen epoch, τ . The constant velocity offsets, C_j , are a location parameter, so the natural choice for an uninformative prior is uniform in C_j . We have already discussed the choice of priors for σ_+ in §2.4. Formally, these priors for $\log P_p$, $\log K_p$, are C_j are improper, i.e., non-normalizable. We solve this by imposing sharp limits on these parameters, $\log P_{\min} \leq \log P \leq \log P_{\max}$, $\log K \leq \log K_{\max}$, and $C_{\min} \leq C \leq C_{\max}$. The choice of limits can be based on other physical constraints (e.g., ability of planet to survive at very short/long orbital periods, a sufficiently massive companion could be detected in the spectra of the primary, and the escape velocity from the galaxy). However, in most cases, these limits will be chosen sufficiently far away from the viable solutions that their exact choice will not affect the shape of the posterior distribution, $p(\vec{\theta}|\vec{d}, \mathcal{M})$. While the possibility of arbitrarily small velocity amplitudes prevents a physical justification for a K_{\min} , clearly it is not possible to detect or constrain the orbital parameters of a planet with K much less than the $\sigma_{\text{ave}} = 1/\sum_k \sigma_k^{-2}$ without many observations. We suggest $K_{\min} = K_{0.5}/2$, where $K_{0.5} = \sigma_{\text{ave}} \sqrt{50/(N_{\text{obs}} - N_{\text{param}})}$ approximates the amplitude for which there is a 50% probability of detecting a planet based on the simulations of Cumming (1999). For systems where a planet is clearly detected, the posterior will not be sensitive to our assumptions about the prior for small values of K , but for planets which are marginally detected, this choice may become significant. A reasonable choice of a normalizable prior is a Jeffery’s prior $p(K) = (K + K_o)^{-1} [\log(1 + K_{\max}/K_o)]^{-1}$, where $K_o \simeq K_{0.5}$ (Gregory 2005a). However, if the posterior distribution includes values of $K \simeq K_o$, then one should be particularly careful to check how sensitive any conclusions are to the choice of K_o . If we were to use flat priors with strict limits ($p(\vec{\theta}|\mathcal{M}) \sim 1$), then the posterior distribution, $p(\vec{\theta}|\vec{d}, \mathcal{M})$, is proportional to $p(\vec{d}|\vec{\theta}, \mathcal{M})$. For the remainder of this paper, we use Jefferies priors for K and σ_+ , so

$$p(\vec{\theta}|\vec{d}, \mathcal{M}) \sim \frac{p(\vec{d}|\vec{\theta}, \mathcal{M})}{\sigma_{+,o} + \sigma_+} \prod_p (K_o + K_p)^{-1}, \quad (18)$$

provided that $\log P_{\min} \leq \log P_p \leq \log P_{\max}$, $\log K_p \leq \log K_{\max}$, $0 \leq e_p \leq 1$, $0 \leq \omega_p \leq 2\pi$, $0 \leq M_{o,p} \leq 2\pi$, $C_{\min} \leq C_j \leq C_{\max}$, and $\sigma_+ \leq \sigma_{+, \max}$. In practice, the reported stellar velocities are typically measured relative to the velocity of the star at the time of a template observation (e.g., a high-resolution observation made without an iodine cell), so the magnitude of each C_j should be no more than the amplitude of the radial velocity variations. Since comparable mass stellar binaries would be easily detected by the presence of a second set of spectral lines, $C_{\max} = -C_{\min} = 100$ km/s is certain to include all allowed orbital solutions, including the possibility spectroscopic binaries. In practice, much smaller values of C_{\max} could be adopted (e.g., based on the range of the observed radial velocities). While this might be useful for some analysis algorithms, it is not necessary for the techniques used in this paper.

3.1.1. Comparison to Paper I

In paper I, we used $\vec{v} = (\log P, \log K, e \sin \omega, e \cos \omega, M_o)$ for calculating our Markov chains, so the Markov chains sampled from a posterior distribution which assumed

$$\begin{aligned} p(e \sin \omega, e \cos \omega) & d(e \sin \omega) d(e \cos \omega) \\ &= 1/\pi d(e \sin \omega) d(e \cos \omega) \\ &= p(e, \omega) de d\omega = e/\pi de d\omega \end{aligned} \tag{19}$$

We then used importance sampling to compute posterior distributions which corresponded to the desired priors, $p(e, \omega) = 1/2\pi$ (Gilks et al. 1996). We made this choice in paper I, since taking steps in $e \sin \omega$ and $e \cos \omega$ was more efficient than taking steps in e and ω for low eccentricity systems. However, this choice also decreased the computational efficiency for long period systems where long period and high eccentricity solutions could not yet be fully excluded. In this paper, we will introduce several additional CTPDFs that allow our Markov chains to efficiently jump from one state to another for both low and high eccentricity models, using a single choice of prior. This eliminates the need for importance sampling to correct for originally calculating a Markov chain using a different prior than is desired for making inferences.

3.1.2. Alternative Priors

From the theorist’s perspective, it might be desirable to assume a prior which is uniform in $\log \mu_{\min} = \log(m_{\min}/M_*)$, where m_{\min} is the minimum allowed mass for given values of P , K , e , and M_* and can be determined by setting $\sin i = 1$ in Eqn. 11. However, radial velocity perturbations have a more direct dependence on K , the velocity semi-amplitude than the planetary mass, m . For this reason we have constructed Markov chains using a prior which is based on K .

If it were important to assume a prior based on μ_{\min} , then importance sampling could be applied to an existing Markov chain. The Jacobian of the transformation is $J = (1 + \mu_{\min})/(1 + \mu_{\min}/3)$. Thus, we could weight each state of a Markov chain assuming a prior uniform on $\log P$, $\log K$, and e by J to obtain an estimate of the posterior probability distribution based on a prior which is uniform on $\log P$, $\log \mu_{\min}$ and e . If we desire a sample from the posterior using this alternative prior, then we can apply rejection sampling to the states calculated in the Markov chain based on $\log K$. In practice, $\mu_{\min} \ll 1$ for planetary mass companions, so $J \simeq 1 + 2\mu_{\min}/3 + O(\mu_{\min}^2) \simeq 1$ and there is very little difference. In fact, if the posterior distribution is sensitive to whether the prior is in terms of K or μ_{\min} , then either the companion is of nearly stellar mass or this is an indication that the data are inadequate to constrain either K or μ_{\min} .

A similar method can be used to sample from a prior that is uniform on $\log a_{\min}$ (the semi-major axis if $\sin i = 1$) rather than $\log P$. This transformation has a Jacobian of $J = [2(6 + 3\mu_{\min})][3(6 + 2\mu_{\min})] \simeq 1 + \mu_{\min}/6 + O(\mu_{\min}^2)$. Again, the two priors are very similar for planetary mass companions and

significant differences in the posteriors are either a stellar mass companion or an indication that the data are inadequate to constrain either $\log P$ or $\log a$. While a reasonable argument could be made in favor of either of these priors, we choose to continue using a prior based on $\log P$ for planetary mass companions, as the differences are negligible.

3.2. Adaptive Step Size Algorithm

In Paper I, we computed Markov chains using a wide range of step sizes. We dismissed the possibility of non-convergence by verifying that Markov chains constructed with these widely varying step sizes all resulted in similar posterior distributions. Unfortunately, the rate of convergence depends sensitively on the step sizes chosen, so computing Markov chains with a wide range of step sizes necessarily results in some chains being very inefficient. In this paper, we suggest abandoning the practice of construct multiple chains with widely varying step sizes, in favor of running more chains with an appropriately chosen step size. Theoretical results (which assume $p(\vec{\theta}|\vec{d}, \mathcal{M})$ is normally distributed) suggest that the best choice for each β_μ would result in an acceptance rate of $\simeq 0.44$ (Gelman et al. 2003). This led us to develop an algorithm to automatically optimize the choice of step sizes, $\vec{\beta}$. While the algorithm outlined below has not been carefully optimized, we find that it provides acceptable results.

At first, we guess reasonable values for the step scale parameters, $\vec{\beta}$. We then begin running a Markov chain and monitor the acceptance rates, $\vec{\psi}$, for each type of step separately. We periodically compare each component of $\vec{\psi}$ to the desired acceptance rate, $\psi_o = 0.44$, to determine if the corresponding elements of $\vec{\beta}$ should be altered. We treat update the β_μ when $(\psi_\mu - \psi_o)^2 > s_\mu^2 \psi_o (1 - \psi_o) / N_\mu$, where s_μ^2 is a parameter that determines how frequently β_μ should be updated (s_μ^2 is initially set to 2), and N_μ is the total number of steps taken using that type of step since the last update of β_μ (including repeats of the same state when a proposed step is rejected). When we determine that β_μ is to be updated, we multiply β_μ by $(\psi_\mu / \psi_o)^\phi$, where $\phi = 1$ for $0.5\psi_o < \psi_\mu$, $\phi = 1.5$ for $0.2\psi_o < \psi_\mu \leq 0.5\psi_o$, and $\phi = 2$ for $0.1\psi_o < \psi_\mu \leq 0.2\psi_o$, but we never reduce β_μ by more than a factor of 100. We impose an upper limit of $\beta_\mu = 4\pi$ for angular variables. After updating an element of $\vec{\beta}$ we resume computing a Markov chain from the final state of the Markov chain prior to updating $\vec{\beta}$. Technically, changing any one of the step sizes destroys the Markov property. Therefore, we must not use the previous states in the chain for inference. Nevertheless, it is more efficient to retain the counts of accepted and rejected steps for each step type (that did not have its scale parameter updated). We find that this produces acceptable results, for the purposes of choosing the step sizes. This process is typically repeated several times to determine an efficient choice for each of the scale parameters in $\vec{\beta}$. Any time β_μ is increased and then consecutively decreased (or vice versa), we increment s_μ^2 . We stop adjusting the scale parameters in $\vec{\beta}$ once each ψ_μ is within 10% of ψ_o or the corresponding $\beta_\mu = 4\pi$ for an angular variable.

3.3. Tests for Non-convergence

In Paper I we used the Gelman-Rubin statistics, \widehat{R} , to test for non-convergence of Markov chains and to decide when the Markov chains were suitable for making inferences about the orbital parameters of a particular system. The Gelman-Rubin statistic compares the variance of any quantity, $z(\vec{\theta})$, estimated from each of the individual Markov chains to the variance of the estimates of the mean of $z(\vec{\theta})$ from the different chains. Following Gelman et al. (2003), we consider the quantities z_{ic} that can be calculated from the model parameters at each iteration (indexed by i) of each Markov chain (indexed by c). If we have N_c Markov chains each of length L_c , then we could estimate the mean value of z_{ic} based on each of the Markov chains as

$$\bar{z}_{.c} = \frac{1}{N_c} \sum_{i=1}^{N_c} z_{ic}, \quad (20)$$

and the average of the variances of z_{ic} within each chain as

$$W(z) = \frac{1}{N_c} \sum_{c=1}^{N_c} \frac{1}{L_c - 1} \sum_{i=1}^{L_c} (z_{ic} - \bar{z}_{.c})^2. \quad (21)$$

Similarly, we could estimate the mean value from the entire set of Markov chains as

$$\bar{z}_{..} = \frac{1}{N_c} \sum_{c=1}^{N_c} \bar{z}_{.c}, = \frac{1}{L_c N_c} \sum_{c=1}^{N_c} \sum_{i=1}^{L_c} z_{ic} \quad (22)$$

and the variance of the estimates of the single chain means by

$$B(z) = \frac{L_c}{N_c - 1} \sum_{c=1}^{N_c} (\bar{z}_{.c} - \bar{z}_{..})^2. \quad (23)$$

Then we can estimate the variance of z_{ic} by a weighted average of $W(z)$ and $B(z)$,

$$\widehat{\text{var}}^+(z) = \frac{L_c - 1}{L_c} W(z) + \frac{1}{L_c} B(z). \quad (24)$$

This is an unbiased estimator of $\text{var}(z)$ either if the N_c initial states of the Markov chains were selected from the target distribution or in the limit $L_c \rightarrow \infty$. If the N_c Markov chains were started from a set of states which have a larger variance than the posterior, then $\widehat{\text{var}}^+(z)$ will initially overestimate $\text{var}(z)$, while $W(z)$ will underestimate it, since the individual Markov chains may not yet have enough states for z to explore its whole range. From these quantities, we form an estimate of $\widehat{R}(z)$,

$$\widehat{R}(z) = \sqrt{\frac{\widehat{\text{var}}^+(z)}{W(z)}}, \quad (25)$$

that is the factor by which the scale of the estimate of the distribution $p(z|\vec{\theta}, \vec{d}, \mathcal{M})$ could be reduced by continuing to calculate longer Markov chains (Gelman et al. 2003). As the individual Markov chains approach convergence, $\widehat{R}(z)$ approaches 1 from above. In paper I, we required that $\widehat{R}_\nu \leq 1.1$ for each $\nu \in (\log P, \log K, e \sin \omega, e \cos \omega, M_o, C)$ before using a chain for inference.

3.4. Stopping Criteria

In §4 of this paper, we will present several modifications to the algorithm of Paper I and compare the rates of convergence of Markov chains calculated with different algorithms. To facilitate quantitative comparisons of a large number of Markov chains, we have adopted an algorithmic stopping criteria which we will use to estimate a stopping time, N_{Stop} .

After determining an appropriate set of step sizes, we begin calculating $N_c = 10$ Markov chains for each system to be analyzed. We periodically pause to calculate the Gelman-Rubin statistics, $\widehat{R}(z_\rho(\vec{\theta}))$, for each of several variables indexed by ρ . Since we desire to accurately estimate, N_{Stop} , we initially check after every 100 steps in each variable, but then increase the time between tests so as to maintain approximately 10% precision in the estimate of N_{Stop} . We require that $\widehat{R}(z_\rho) \leq 1.01$ for each ρ . We also calculate an estimate of the effective number of independent draws, $\widehat{T}(z)$,

$$\widehat{T}(z) = L_c N_c \min \left[\frac{\widehat{\text{var}}^+(z)}{B(z)}, 1 \right]. \quad (26)$$

This attempts to correct for the effects of autocorrelation within each of the Markov chains on the total number of states in the Markov chains (Gelman et al. 2003). We require that $\widehat{T}(z_\rho(\vec{\theta})) \geq 1000$ for each quantity that we monitor (labeled by ρ). When all the tests based on both $\widehat{R}(z_\rho)$ and $\widehat{T}(z_\rho)$ are satisfied, we set N_{Stop} to be the number of steps in each Markov chain at this time.

Since we repeatedly test our Markov chains with these criteria, there is an increased chance that the values of \widehat{R} and \widehat{T} will fluctuate below our thresholds by chance. Therefore, once both criteria are met, we then continue computing the Markov chains to increase the length of the Markov chains by approximately 1%, 2%, 3%, 4% and 5%. and repeat all the tests at each of these times. If the criterion for any one of the $\widehat{R}(z_\rho)$ or $\widehat{T}(z_\rho)$ are not met at any of these times, then we discard the tentative value of N_{Stop} and continue computing each of the Markov chains. Therefore, our final stopping criteria requires $\widehat{R}(z_\rho)$ and $\widehat{T}(z_\rho)$ satisfy the above criteria for all quantities labeled by ρ at all five consecutive tests, but we report the number of steps before the first of the five consecutive set of passed tests.

Special care is required for applying the Gelman-Rubin test to variables which are angles. If the mean values of a variable in two chains are ϵ and $2\pi - \epsilon$, then the difference between the mean values should be 2ϵ not $2\pi - 2\epsilon$. Similarly, care must be taken when calculating the variance of an angular variable within a Markov chain not to overestimate the variance due to the particular representation of the angle. To circumvent this problem, for any angle, ξ , we use the mean and variance of a “standardized” angle, ξ_{std} . First, we define the notation $\{\xi\}$ to be a representation of the angle ξ that lies in the interval $[-\pi, \pi)$. We consider the values of $\{\xi - w\pi/8\}$, where w ranges from 0 to 15, and calculate their mean, $\overline{\{\xi - w\pi/8\}}$, and variance, $\text{var}(\{\xi - w\pi/8\})$. We then set w^* to be value of w which minimizes $\text{var}(\{\xi - w\pi/8\})$, and obtain an initial estimate for the mean standardized angle, $\bar{\xi}_{std,1} \equiv w^*\pi/8 + \overline{\{\xi - w^*\pi/8\}}$. We then compute the mean and variance of $\{\xi - \bar{\xi}_{std,1}\}$ to determine our final estimates of the standardized mean $\bar{\xi}_{std} \equiv \bar{\xi}_{std,1} + \{\xi - \bar{\xi}_{std,1}\}$

and the standardized variance, $\text{var}(\xi_{\text{std}}) \equiv \text{var}(\xi - \bar{\xi}_{\text{std},1})$ Note, that it is important to use a two pass method to calculate these variances.

If we were constructing these Markov chains for the purpose of inference we would not calculate the values of \hat{R} so frequently or stop our Markov chains as soon as this criteria were satisfied. We do not claim that this set of tests is sufficient to proof convergence. Indeed, it is impossible to prove convergence and only possible to prove non-convergence. Therefore, the standard practice is to perform multiple tests for non-convergence until one is satisfied that the Markov chain is sufficiently close to convergence to be used for inference (Gelman et al. 2003). The above stopping criteria is one example of such a suite of tests for non-convergence. We believe that the above set of tests provides an adequate means of quantitatively assessing the efficiency of the various CTPDFs which we explore in §5.

4. Improving the Efficiency of MCMC

The computational efficiency of the basic MCMC algorithm presented in Paper I was typically limited by high correlations between some model parameters. One obvious strategy for improving the efficiency of MCMC would be to perform a principal components analysis (PCA) of the states from a preliminary Markov chain and to perform a rotation from the original model parameters to a set of principal axes based on the preliminary Markov chain. If the preliminary Markov chain were representative of the full posterior distribution and it were possible to find a linear transformation from the model parameters to an efficient basis for taking steps in a Markov chain, then this would be a good strategy. We have attempted this method, but found less than satisfactory results. In particular, the length of the preliminary Markov chain necessary for accurately estimating the best linear transformation can be so long that we do not achieve our goal of reducing the necessary computations. This is related to the observation that even the best linear combination of model parameters often does not provide an efficient basis, due to the non-linear nature of the Keplerian model. For example, for planets with an orbital period comparable to the duration of observations, there is often a large non-linear degeneracy between the orbital period and eccentricity. Therefore, we found that a PCA-type analysis could be useful for identifying and removing linear correlations, but it is not sufficient for improving the efficiency of MCMC due to non-linear correlations. Instead we find that such PCA-type analyses are more useful for providing intuition that can help guide the choice of alternative CTPDFs.

4.1. Alternative Choices for the Candidate Transition Probability Function

We have developed a more general method of generating CTPDFs which is capable of removing both linear and non-linear correlations. One simple way of generating alternative CTPDFs is to identify combinations of model parameters ($\vec{u}(\vec{\theta})$) which may be better or more poorly constrained

by the observational data than the model parameters ($\vec{\theta}$). A CTPDF can be constructed by making a change of variables, taking a step which is Gaussian in the transformed variables, and changing back to the original set of model parameters. By using the Metropolis-Hastings algorithm the Markov chain will still be reversible and still converge to the same distribution as if steps were taken in the original variables. For the acceptance probability in Eqn. 5, the function $q(\vec{\theta}|\vec{\theta}')$ is proportional to $J = \left| \partial \vec{u}(\vec{\theta}) / \partial \vec{\theta} \right|$, the magnitude of the determinant of the Jacobian of the transformation between $\vec{\theta}$ and $u(\vec{\theta})$. Below we present several examples of CTPDFs which can speed convergence for some planetary systems and observational data sets.

4.2. Orbital Period and Phase

The mean anomaly at time t is given by

$$M(t) - M_o = \frac{2\pi}{P} (t - \tau) \quad (27)$$

where M_o is a constant model parameter, the orbital phase at $t = \tau$. Consider the case where the observational data constrain the mean anomaly at $t = \tau'$ better than at $t = \tau$. In that case, a sensible choice for \vec{u} might include the variable

$$M'_o \equiv M(\tau') = M_o + \frac{2\pi}{P} (\tau' - \tau). \quad (28)$$

This generates an obvious CTPDF with the form of Eqn. 7 using the variable $u_{M'_o}(\vec{\theta}) = M'_o$. If $\vec{\theta}_{-M_o}$ (all the variables in the state excluding M_o) are held constant, but M_o is forced to change to satisfy Eqn. 28, then M'_o is related to M_o by a simple linear shift. A CTPDF based on this type of step in M'_o will be just as efficient as one based on M_o .

The use of M'_o can also lead to another new CTPDF involving the orbital period. We can take a step which alters both M_o and $\log P$ while holding M'_o constant. Due to the constraint, there is still only one degree of freedom in this step, so we can still use Eqn. 7, adding only one new step scale parameter to $\vec{\beta}$. The change of variable results in a Jacobian equal to unity and hence the ratio $q(\vec{\theta}|\vec{\theta}')/q(\vec{\theta}'|\vec{\theta}) = 1$ in Eqn. 5 for both these new step types.

Since we have assumed that the observations constrain M'_o more tightly than M_o , the pair P and M_o is more highly correlated than the pair P and M'_o . The lower correlation will cause a Markov chain to converge more quickly when taking steps in $\log P$ while holding M'_o constant rather than taking steps in $\log P$ while holding M_o constant. To understand why taking steps in $\log P$ with constant M_o would slow the rate of convergence, let us assume that the variances of the marginal posterior distributions of $\log P$, M'_o and M_o are $\sigma_{\log P}^2$, $\sigma_{M'_o}^2$ and $\sigma_{M_o}^2$, with $\sigma_{M'_o}^2 < \sigma_{M_o}^2$. If a step in $\log P$ is of size $\Delta \log P$, then the implicit step in M_o (M'_o) while holding M'_o (M_o) constant will be of size $\simeq 2\pi(\tau' - \tau)\Delta \log P/P$. If $(\tau' - \tau)/P$ is large, then the implicit change in the mean anomaly at $t = \tau$ (τ') will often be larger than $\sigma_{M'_o}$, resulting in a large fraction of

trial states being rejected. In order to maintain a reasonable acceptance rate, the typical trial step sizes $\beta_{\log P}$ will need to be reduced from $\simeq \sigma_{\log P}$ to $\simeq \sigma_{M'} P \Delta \log P / (2\pi \Delta t)$. However, the smaller value of $\beta_{\log P}$ will mean that the Markov chain requires more steps to explore the allowed range of orbital periods. If $\beta_{\log P} \ll \sigma_{\log P}$, then the Markov chain will behave like a random walk, requiring a factor of $\sim (\sigma_{\log P}^2 / \sigma_{M'}^2) (4\pi^2 \Delta t^2 / P^2)$ more steps to explore the allowed range of orbital periods and initial mean anomalies by stepping in $\log P$ while holding M_o fixed than if stepping in $\log P$ while holding M'_o fixed.

In order to minimize the correlation between $\log P$ and $M(\tau')$ and to maximize the efficiency of our Markov chains, we want to choose τ' to be the time at which the mean anomaly is best constrained. Unfortunately, in practice we do not know the time at which $M(t)$ is best constrained *a priori* and must make a reasonable approximation. Clearly, one should not hold $M(t)$ constant for a time well before or after all the observations. A much better initial guess would be the weighted average of the observation times,

$$\tau' = \frac{\sum_k t_k \sigma_k^{-2}}{\sum_k \sigma_k^{-2}} \quad (29)$$

where t_k is the time of the k th observation and σ_k is the uncertainty in the k th observation. We have found this to be a good initial guess for many practical radial velocity data sets. If after running a Markov chain it becomes clear that there is a significant correlation between $\log P$ and M_o , then one could estimate a better guess from the current Markov chain and start over with a new choice for τ' .

In this simple example, we could have simply chosen a different epoch for defining our orbital parameters (i.e., set $\tau = \tau'$). Indeed, for the remainder of the paper, we will simply use M_o assuming that τ has been chosen wisely. Nevertheless, we include this methodical explanation to introduce our approach of using alternative choices for CTPDFs. Additionally, this complete development allows for τ' to be a function of the model parameters at each state in the Markov chain. This may be useful for systems when we include a noise source of unknown magnitude and the values of σ_k depend on the model parameter σ_+ . If the posterior distribution permits a wide range of σ_+ , then the time at which the mean anomaly is best constrained may vary from model to model in a Markov chain and it may be advantageous to recalculate τ' based on Eqn. 29 after each step in σ_+ to further improve the efficiency of the Markov chain. However, in our experience, the practical differences are typically small for data sets where σ_+ is small and the values $\sigma_{k,obs}$ are similar.

4.3. $\omega + M_o$ and $\omega - M_o$

For planets in low eccentricity orbits the longitude of pericenter can be poorly constrained. If the observations are consistent with $e = 0$ and Markov chain takes steps in e and ω , then the Markov chain would need to explore the entire range of ω . If β_ω is small compared to 2π (e.g., due to correlation with another model parameter), then the chain will be slow to converge. Since the initial mean anomaly is related to the time since pericenter, the initial mean anomaly can only

be well constrained when the argument of pericenter is also well constrained. When neither ω or M_o are well constrained individually, the observational data can often better constrain $\omega + M(\tau)$ or $\omega + T(\tau)$, the angular position of the star relative to the plane of the sky at time, τ . The true anomaly T is related to the mean anomaly via Eqns. 9 & 10. While the relationship between $M(t)$ and $T(t)$ is transcendental, we can approximate T with a series expansion in e ,

$$T \simeq M + 2e \sin M + \frac{5}{4}e^2 \sin 2M + O(e^3). \quad (30)$$

For low eccentricity systems, $T \simeq M$ and we find it advantageous to use CTPDFs which are based on the variables $\omega + M_o$ and $\omega - M_o$. Clearly a prior which is uniform in the angles ω and M_o is also uniform on the angles $\omega + M_o$ and $\omega - M_o$. By using a transition probability function based on Eqn. 12 and the variables $\omega + M_o$ and $\omega - M_o$, the Markov chain is able to use a small scale, $\beta_{\omega+M_o}$, for steps in $\omega + M_o$ and a larger scale, $\beta_{\omega-M_o}$, for steps in $\omega - M_o$, since this choice of variables has a much lower correlation. We have found that this simple choice can greatly speed convergence for low eccentricities and can also be useful for systems with significant eccentricities.

4.4. $e \sin \omega$ and $e \cos \omega$

As discussed above, the argument of pericenter is typically not well constrained for planets in low eccentricity orbits. In Paper I, we addressed this issue by using the variables $e \sin \omega$ and $e \cos \omega$. This works well for low eccentricity systems, since the Markov chain can jump to arbitrary values of ω in a just one or two steps when $e \simeq 0$. One disadvantage of this approach is that a uniform prior in $e \sin \omega$ and $e \cos \omega$ results in a non-uniform prior for e . In Paper I a Markov chain was run with $p(e) = e$ and then importance sampling was used to resample assuming a prior uniform in e . This typically worked well for low eccentricity systems. However, it required calculating longer Markov chains and checking that the posterior distributions were sufficiently similar for importance sampling to provide accurate results. For some systems where the eccentricity was poorly constrained, the method of Paper I resulted in the Markov chain spending a larger than necessary amount of time exploring high eccentricities and significantly reduced the efficiency of the Markov chain. Therefore, we now prefer to sample directly from a prior that is uniform in e . It is trivial to take steps in e (holding ω constant) and ω (holding e constant).

In order to explore parameter space quickly for low eccentricity systems, we introduce two new CTPDFs based on Eqn. 7 and the variables $e \sin \omega$ and $e \cos \omega$. We generate a trial state by taking a step in $e \sin \omega$ and holding $e \cos \omega$ fixed or by taking a step in $e \cos \omega$ and holding $e \sin \omega$ fixed. The MH algorithm is used to generate a reversible CTPDF and guarantee that the Markov chain will still converge to the same $p(\vec{\theta}|\vec{d}, \mathcal{M})$ as it would if only taking steps in e and ω .

Given the domains of e and ω ($0 \leq e \leq 1$ and $0 \leq \omega \leq 2\pi$), it is easy to see geometrically that a uniform prior in $e \sin \omega$ and $e \cos \omega$ would correspond to a prior in e and ω which is proportional to e . Therefore, when comparing the current state to a candidate state generated by stepping in

the variable $u_{e \sin \omega}$ or $u_{e \cos \omega}$, the acceptance rate should decrease the probability of accepting the model with the larger eccentricity. More formally, Eqn. 19 shows that the the Jacobian of the transformation is $J = e$. Therefore, when taking steps in $e \cos \omega$ and $e \sin \omega$ rather than e and ω , the ratio used in Eqn. 5 of the MH algorithm

$$\frac{q(\vec{\theta}|\vec{\theta}')}{q(\vec{\theta}'|\vec{\theta})} = \frac{e}{e'} \quad (31)$$

is not a constant as it has been for previous CTPDFs.

Note that we have not yet completely specified the types of steps to be taken. Each time we change either $e \sin \omega$ or $e \cos \omega$, we implicitly change other quantities, such as e , ω , and $\omega + M_o$. If the quality of the orbital fit depends sensitively on one of these quantities, then there is likely to be another case of correlated variables and inefficient sampling of the posterior. Our simulations have shown that stepping in $e \sin \omega$ and $e \cos \omega$ while holding P , K , and $\omega + M_o$ fixed is typically a good choice.

4.5. $\omega \pm T_o$

For systems with a significant eccentricity, $(T(t) - M(t))/2\pi \ll 1$, so it may be preferable to take steps using the variables, $\omega + T(\tau)$ and $\omega - T(\tau)$ while holding the other fixed. Differentiating Eqns. 9 & 10, we find

$$\frac{dT}{dM} = \frac{\sqrt{1 - e^2}}{(1 - e \cos E)^2}, \quad (32)$$

and the Jacobian of the transformation from ω and M_o to $\omega \pm T_o$ is $J = \left| 2\sqrt{1 - e^2}(1 - e \cos E)^{-2} \right|$. Again, we use a CTPDF based on Eqn. 12 with the acceptance probably in Eqn. 5 given by

$$\frac{q(\vec{\theta}|\vec{\theta}')}{q(\vec{\theta}'|\vec{\theta})} = \frac{\sqrt{1 - e^2} (1 - e' \cos E'(\tau))^2}{\sqrt{1 - e'^2} (1 - e \cos E(\tau))^2}. \quad (33)$$

We find that the use of these steps can be useful for high eccentricity systems.

4.6. Time of Pericenter

When the time span of observations of an eccentric planet are comparable to the orbital period, the time of pericenter may be more tightly constrained by the observations than the initial mean anomaly. Additionally, the correlation between the orbital period and initial mean anomaly may still slow convergence. By allowing steps in $T_p = \tau - PM(\tau)/(2\pi)$ (holding $\log P$ fixed), it may be possible to speed convergence. The Jacobian of the transformation from P and M_o to P and T_p is simply $J = |P/(2\pi)|$, so we use a transition acceptance probability of

$$\frac{q(\vec{\theta}|\vec{\theta}')}{q(\vec{\theta}'|\vec{\theta})} = \frac{P}{P'} \quad (34)$$

in Eqn. 5 to generate a reversible CTPDF.

4.7. $1/P$

If there is a large range of possible orbital periods, then it can be advantageous to take smaller steps when at short periods and larger steps when at long periods. While using $\log P$ results in a step size scale that is proportional to the period, the scale for a change in the orbital period to affect the velocities by a given amount increases even faster, $\beta_{\log P} \sim P$. Therefore, it can be advantageous to take steps using Eqn. 7 using $u_{1/P}(\vec{\theta}) = 1/P$ with a step size scale, $\beta_{1/P}$. Gregory (2005b) suggested a similar optimization, but did not give details. When replacing steps in $\log P$ with steps in $1/P$, the acceptance probability for use in Eqn. 5 is

$$\frac{q(\vec{\theta}|\vec{\theta}')}{q(\vec{\theta}'|\vec{\theta})} = \frac{P'}{P}. \quad (35)$$

We find that this is particularly helpful for planets with a large range of acceptable orbital periods. This can occur for multimodal posterior distributions (Gregory 2005a) or when the orbital period is comparable to the duration of observations (Ford 2005a).

4.8. $K \cos \omega$ & $K \sin \omega$

The radial velocity perturbation of a planet on a Keplerian orbit can be written as a linear function of the variables $K \cos \omega$ and $K \sin \omega$, if the orbital elements P , e , and M_o are held fixed. This led us to consider CTPDFs based on the variables $u_{K \cos \omega}(\vec{\theta}) = K \cos \omega$ and $u_{K \sin \omega}(\vec{\theta}) = K \sin \omega$. When replacing steps in $\log K$ and ω with steps in $K \cos \omega$ and $K \sin \omega$, the acceptance probability for use in Eqn. 5 is

$$\frac{q(\vec{\theta}|\vec{\theta}')}{q(\vec{\theta}'|\vec{\theta})} = \frac{K^2}{K'^2}. \quad (36)$$

Our tests found that these steps could be useful for long period planets.

4.9. $\log(K\sqrt{1-e})$ & $\log(K/\sqrt{1-e})$

When a planet’s orbital period is comparable to the duration of observations, then there can be significant degeneracies between the orbital parameters. From studying the posterior distribution of dozens of long period systems, we recognized that for such systems $\log(K\sqrt{1-e})$ and $\log(K/\sqrt{1-e})$ often have lower correlations with the other orbital parameters than K and e individually. Therefore, we considered taking steps in these variables. When replacing steps in $\log K$ and e with steps in $\log(K\sqrt{1-e})$ and $\log(K/\sqrt{1-e})$, the acceptance probability for use in Eqn.

5 is

$$\frac{q(\vec{\theta}|\vec{\theta}')}{q(\vec{\theta}'|\vec{\theta})} = \frac{|1 - e'|}{|1 - e|}. \quad (37)$$

We found that taking steps in $K/\sqrt{1-e}$ while holding $K\sqrt{1-e}$ could be useful for long period planes.

4.10. Other Variables

We have also considered taking steps in the numerous combinations of variables $P(1-e)^{3/2}M_*^{1/2}$, $P^{2/3}(1-e)M_*^{1/3}$, $P^{2/3}(1+e)M_*^{1/3}$, $Ke \cos \omega$, $K\sqrt{1-e^2}$, $K/\sqrt{1-e^2}$, $K\sqrt{1-e}$, and $\omega + 2M_o$. While some of these have helped particular systems, we have not found these other quantities to be advantageous in general. Therefore, we suggest monitoring the correlations among all model parameters, $\vec{\theta}$, all variables being used for steps $\vec{u}(\vec{\theta})$, and additional variables such as those above. If statistics such as \hat{R} and \hat{T} indicate the Markov chains are converging slowly for any of these variables, then we suggest examining the correlations between all pairs of monitored variables to see if additional CTPDFs may be useful for improving the rate of convergence.

4.11. Directly Sampling from Conditional Posterior Distribution

For some variables it is possible to directly sample from the conditional posterior distribution without resorting to Metropolis-Hastings algorithm. This reduces the autocorrelation of a Markov chain, and hence increases the rate of convergence. Unfortunately, if there are significant correlations between various model parameters, then the Markov chain will still tend to have a significant autocorrelation.

For example, the radial velocity predicted by the model is a linear function of each of the constant velocity terms, C_j . By assuming a normal prior for C and taking the limit as the variance goes to infinity, we can compute the conditional posterior for the constant terms assuming a uniform prior (Bullard, private communications). We find that the conditional posterior for the new constant terms C_j given the data (\vec{d}) and the model parameters excluding C_j ($\vec{\theta}_{-C_j}$) is given by $p(C_j|\vec{d}, \vec{\theta}_{-C_j}, \mathcal{M}) \sim N(C'_j, \sigma_{C'_j}^2)$ where

$$C'_j = \frac{\sum_k \left(d_k - v_{*,\vec{\theta}}(t_k, j_k | \vec{\theta}_{-C_j}, C_j = 0, \mathcal{M}) \right) \sigma_k^{-2} \delta_{j_k, j}}{\sum_k \sigma_k^{-2} \delta_{j_k, j}}, \quad (38)$$

$\sigma_{C'_j}^2 = \left(\sum_k \sigma_k^{-2} \delta_{j_k, j} \right)^{-1}$, and $\delta_{j_k, j}$ is the Kronecker delta.

4.12. Numerical Tests

We have constructed numerous simulated data sets for testing the efficiency of Markov chains using various CTPDFs. Here we concentrate on quality data sets that provide significant constraints on the orbital parameters. We intentionally do not consider data sets where a planet is only barely detected due to a small amplitude or a small number of observations, as these can result in multi-modal posterior distributions (Gregory 2005a) and even the optimizations presented in this paper can struggle with multi-modal posterior distributions. Our simulated data sets assume $\simeq 80$ observations each with an observational uncertainties of $\sigma_{k,obs} \simeq 1\text{m s}^{-1}$. We include a planet causing a wobble of $K \simeq 50\text{m s}^{-1}$, typical for an extrasolar giant planet. We include jitter as a Gaussian noise source with $\sigma_+ = 2\text{m s}^{-1}$, so that $K/\sqrt{\sigma_{k,obs}^2 + \sigma_+^2} \simeq 20$. We consider several orbital periods ranging from 1/30 - 1 times the time span of the observations. The observation times and uncertainties are based on actual observation times and uncertainties from the California and Carnegie planet search. We then calculated many Markov chains for each data set using various sets of CTPDFs to determine which result in the most rapid rate of convergence. We use these simulations to compare the performance of various CTPDFs. We present the median stopping time for several choices of CTPDFs in Table 2. The first two columns show the results for the CTPDFs very similar to those used in Paper I.

$$\vec{u}_1(\vec{\theta}) = (\log P, \log K, e, \omega, M_o, C, \sigma_+), \quad (39)$$

$$\vec{u}_2(\vec{\theta}) = (\log P, \log K, e \sin(\omega), e \cos(\omega), M_o, C, \sigma_+), \quad (40)$$

The remaining columns show the results for some of the best CTPDFs developed in this paper. Note that the new CTPDFs often accelerate convergence by one to nearly three orders of magnitude. These CTPDFs make it practical to perform Bayesian analyses of many single planet systems with only $\sim 10^4$ steps (using the strict stopping criteria from §3.4. Even for a planet with an orbital period equal to the duration of the observations and a large eccentricity, we find stopping times of $\sim 10^6$ steps. Thus, these optimizations presented in this paper, make it practical to perform Bayesian analyses of the vast majority of extrasolar planets. For reference, we find that the computer time required is $\sim 8 \times 10^{-7} N_{obs} N_p L_c N_c$ seconds using a 3GHz Intel CPU, where N_{obs} is the number of observations, N_p is the number of planets, L_c is the number of states in each chain, and N_c is the number of chains, if the planets are assumed to be on non-interacting Keplerian orbits. While this study used $N_c = 10$ chains to ensure accurate estimates for the stopping time, experience has shown that $N_c \simeq 5$ would be sufficient for most applications.

4.13. Recommendations

We now offer some simple recommendations that can be generally implemented. We find that the optimal set of CTPDFs depends on the types of orbital solutions consistent with the observational data. In particular, the optimal choice depends on the range of allowed eccentricities.

Since the purpose of MCMC is to determine the allowed range of orbital parameters, it may not be clear which set of CTPDFs should be used. In these cases, we suggest alternating between the various types of CTPDFs suggested below. While this is less efficient than using only the CTPDF most appropriate for the particular planet, it is also more robust. Of course, preliminary analyses often provide a good indication of whether the eccentricity is likely to be small or large. If it is clear that the eccentricity can not be large, then it would be more efficient to use the CTPDFs suggested in §4.13.1.

4.13.1. Low Eccentricity Orbits

For systems with low eccentricities, we find that taking steps in the set of model parameters,

$$\vec{u}_3(\vec{\theta}) = (1/P, \log K, e \sin(\omega), e \cos(\omega), \omega + M_o, C, \sigma_+), \quad (41)$$

results in good performance. Note that when we step in $e \sin(\omega)$ or $e \cos(\omega)$, we hold $\omega + M_o$ constant. The Jacobian of the transformation relating $\vec{u}_3(\vec{\theta})$ to $\vec{\theta}$ is $J_1 = e/P$. When taking Metropolis-Hasting steps, we use the ratio of the Jacobians of the two states

$$\frac{q(\vec{\theta}|\vec{\theta}')}{q(\vec{\theta}'|\vec{\theta})} = \frac{eP'}{e'P} \quad (42)$$

as the acceptance probability in Eqn. 5 to ensure that the Markov chains converge to the desired posterior distribution.

Using CTPDFs based on \vec{u}_3 , we found that Markov chains were typically suitable for inference after $\sim 10^{4-4.5}$ steps when analyzing data for a planet with a moderate eccentricity ($e = 0.5$) and an orbital period longer than duration of observations. For an orbital period equal to the duration of observations, $\sim 10^{4.7}$ steps were needed. For very small eccentricities, $\sim 10^{4.6-5.4}$ steps were needed. Even for systems with large eccentricities, $\sim 10^{5-7}$ steps were needed. These results indicate that this set of CTPDFs is very efficient for nearly circular orbits and also works across a broad range of eccentricities. However, the reduction in efficiency for high eccentricity and long period systems has motivated us to test other sets of CTPDFs to further improve the efficiency for such systems.

4.13.2. Long Period & High Eccentricity Orbits

For systems with high eccentricities, we find that alternating between taking steps in \vec{u}_3 and two additional sets of model parameters,

$$\vec{u}_4 = (P^{-1}, K \sin(\omega), K \cos(\omega), e, \omega + T_o, C, \sigma_+), \text{ and} \quad (43)$$

$$\vec{u}_5 = (P^{-1}, \log [K\sqrt{1-e}], \log [P(1-e)^{3/2}], \omega, T_p, C, \sigma_+) \quad (44)$$

is advantageous. The Jacobians for these transformations are $J_4 = \left| K^2 \sqrt{1 - e^2} P^{-1} (1 - e \cos E(\tau))^{-2} \right|$ and $J_5 \sim 1/|1 - e|$. This combination of CTPDFs provides a modest improvement for planets with a moderate eccentricity, and is particularly useful for high eccentricities. Using this combination, the stopping times for high eccentricity systems were reduced to $\sim 10^{4.7-6}$ steps, provided that orbital period is less than 80% of the duration of observations. Even for the most challenging cases considered ($e = 0.8$ and $T_{obs}/P = 1 - 1.25$, where T_{obs} is the time span of observations), Markov chains computed with these CTPDFs satisfied the stopping criteria from §3.4 after $\sim 10^{6.2-6.4}$ steps.

5. Multiple Planet Systems

So far the transition probability functions presented all involve the orbital parameters of only a single planet. Nevertheless, these refinements are very valuable when applying MCMC to multiple planet systems. Since the correlations between orbital parameters for different planets are often small, convergence towards the posterior distribution of orbital parameters for the entire system can be dramatically accelerated by using CTPDFs that allow the Markov chains to explore the full range of allowed orbital parameters for each planet efficiently.

5.1. Monitoring Dynamically Significant Quantities

It is likely that additional optimizations are possible for multiple planet systems. However the significant diversity of planetary systems means that there is an enormous array of potentially useful choices for the CTPDFs. We hope that the methods explained in this paper and the examples provided will make it straightforward for researchers to construct transition probability functions which are appropriate for the particular problem at hand and converge to the desired posterior probability distribution. Here, we point out a few dynamically significant quantities that should at least be monitored when testing the Markov chain for non-convergence. In some cases, these combinations may also be useful for including in the set of variables used for CTPDFs.

5.1.1. Secular Evolution

For multiple planet systems dynamical stability may make it possible to constrain the orbital inclination, i , and the longitude of ascending node, Ω (see §5.2). In particular, the secular evolution of a multiple planet system is often qualitatively different when the relative inclination, i_{rel} , is between 40° and 140° . Indeed, often such large relative inclinations can be excluded by imposing the requirement of long-term dynamical stability, even if $\sin i \ll 1$ for both planets. It is important to remember that the relative inclination of two planets (labeled in and out) is not simply the

difference of the inclinations to the line of sight, but depends on the ascending nodes,

$$i_{rel} = \cos i_{in} \cos i_{out} - \sin i_{in} \sin i_{out} \cos(\Omega_{in} - \Omega_{out}). \quad (45)$$

Depending on the regime, the secular inclination evolution can also be sensitive to $\Delta\Omega = \Omega_{out} - \Omega_{in}$, $\Delta\varpi = \varpi_{out} - \varpi_{in} = \Omega_{out} + \omega_{out} - \Omega_{in} - \omega_{in}$, e_{in} , and e_{in}/e_{out} .

We recommend monitoring $\Delta\omega$ and $\log(e_{in}/e_{out})$ for all multiple planet systems to ensure that any Markov chain used for inference displays adequate mixing of these variables. When including additional constrains such as dynamical stability, we also recommend monitoring $\Delta\Omega$, $\Delta\varpi$, and i_{rel} . Such monitoring is important for establishing the suitability of Markov chains for inference about the secular evolution of multiple planet systems, as done in Ford et al. (2005) where $\omega_{in} - \omega_{out}$ and $\omega_{in} + \omega_{out}$ were also used as the basis for CTPDFs.

5.1.2. Evolution near a Mean Motion Resonance

If the two planets are near a low order mean motion resonance, then it is dynamically interesting to monitor the resonant variables. In particular, it is of interest if these angles are librating or circulating and, if librating, what their amplitude is. For example, in a nearly coplanar system with two planets near a 2 : 1 mean-motion resonance (e.g., GJ 876), the lowest order eccentricity mean motion resonances variables are $\varphi_1 = \varpi_{in} + M_{in} - 2M_{out}$ and $\varphi_2 = \varpi_{out} + M_{in} - 2M_{out}$. Since these quantities vary over an orbital timescale, it is important to monitor these variables at an epoch where they are relatively well constrained. If the system is librating, their amplitude of libration also depends on $2P_{in}/P_{out}$. Therefore, we recommend monitoring the variables φ_1 , φ_2 , and $\log(2P_{in}/P_{out})$, in addition to the variables related to the secular evolution of the system.

5.2. Dynamical Constraints & Importance Sampling

In multiple planet systems, the requirement that the planetary system be dynamical stable (for some time, t_{max} , which is less than or equal to the age of the system) can place significant constraints on orbital parameters. Unfortunately, performing long-term n-body integrations can require a substantial amount of computer time. MCMC can be used to improve the computational efficiency of dynamical stability studies. MCMC can be used to estimate a posterior probability distribution for the orbital parameters which incorporates only knowledge from the observations data (and not the requirement of dynamical stability). Then, that posterior distribution can be used as the the initial conditions for the n-body integrations to test for dynamical stability. Initial conditions which result in dynamical instability are rejected, while initial conditions which are found to be stable for t_{max} are accepted for inclusion in a posterior probability distribution which includes both the observational and dynamical constraints. This technique can be particularly useful for

efficiently constraining the inclination of a planet’s orbit to the line of sight, i , the ascending node, Ω , and the relative inclination of the orbital planets of two planets, i_{rel} .

Note that it is computationally advantageous to first calculate a posterior distribution based on the observational data alone and use this distribution as the initial conditions for a series of integrations to test for their long-term stability (requiring $\sim 10^4\text{--}10^6$ yr integrations). When calculating the posterior distribution based on the observational data alone, the integrations only need to last for the duration of observations (e.g., $\sim 1\text{--}10$ yr). When testing the long-term stability, much longer integrations are typically required (e.g., $\sim 10^4\text{--}10^6$ yr). Therefore, separating these two dramatically reduces the total length of integrations necessary, and the final estimate of the posterior distribution (including both observational and dynamical constraints) is still accurate, provided that there is significant overlap between the posterior based on observations only and the set of solutions satisfying the dynamical constraints. An additional improvement in computational efficiency is possible, since the length of the Markov chain for calculating the posterior based solely on observational data can be orders of magnitude greater than the number of initial conditions for the long integrations to test dynamical stability. By selecting a small subset of states from a much longer Markov chain, we can virtually eliminate the correlation between the sets of initial conditions used for long-term integrations, reducing the number of long integrations necessary to accurately characterize the long-term stability.

In many multiple planet systems, the mutual planetary perturbations are negligible over the timescale of the observational data, even if they may be significant on secular timescales (e.g., ν Andromedae, 47 UMa). In these cases, the Markov chains described in §5.2 can be calculated assuming that each planet is on an independent Keplerian orbit. When this is a good approximation the necessary computation time is greatly reduced, as the direct integration of the few-body problem for the duration of observations can be replaced by solving the Kepler equation for each planet at each observation time.

We can further improve the accuracy of this approximation by first calculating the posterior distribution for model parameters assuming a likelihood function based on the approximation of independent Keplerian orbits. A subset of the states from the Markov chains using the approximate model can then be used as the initial conditions for direct n-body integrations, and importance sampling can be used to calculate weights for each set of initial conditions. It is possible to obtain a sample from the actual posterior distribution (based on the observations and direct n-body integrations) using these initial conditions, weights, and rejection sampling. This sample can then be used as the initial conditions for long-term integrations to impose the requirement of long-term dynamical stability.

One concern with this method is that if the observations constrain parameters more tightly in the approximate model than in the full model, then this two-stage method could underestimate the uncertainty of the parameters in the full model. This can be avoided by altering the target distribution for on the approximate model, so that it is broader than the posterior distribution

based on the full model. We propose two ways to make such a modification. Instead of initially calculating Markov chains with a target distribution equal to the posterior of the approximate model, $p(\vec{\theta}|\vec{d}, \mathcal{M}) \sim p(\vec{\theta}, \mathcal{M})p(\vec{d}|\vec{\theta}, \mathcal{M})$, we can calculate Markov chains with a target distribution equal to $p(\vec{\theta}|\vec{d}, \mathcal{M}) \sim p(\vec{\theta})p(\vec{d}|\vec{\theta}, \mathcal{M})^\gamma$. By setting $\gamma < 1$, we can choose the target distribution to be broader than the posterior distribution in the approximate model. An alternative method is to artificially increase the estimates of the measurement errors when calculating the approximate model, $\sigma^2(t_i) \leftarrow \sigma^2(t_i) + \sigma_a^2$. We prefer this method when a good estimate for σ_a^2 is available, so the value for σ_a^2 can be chosen based on the magnitude of the expected deviations from independent Keplerian orbits. This method was applied and tested for the analysis of the ν Andromedae system in Ford et al. (2005).

6. Example Applications

In this section we demonstrate the improvements in efficiency of MCMC on several actual extrasolar planet systems. We include one particularly interesting short-period planet, one recently announced long-period planet, one slowly interacting multiple planet system, and one rapidly interacting multiple planet system.

6.1. HD 209458

The transiting planet around HD 209458 has provoked considerable interest on account of its large radius (Brown et al. 2001). Bodenheimer, Laughlin & Lin (2003) offered a potential explanation, namely that the radius could be inflated due to tidal heating if the planet still had an eccentricity of $\simeq 0.03$. Additional radial velocity observations allowed radial velocities to impose a stronger constraint on the allowed range of eccentricities (Laughlin et al. 2005). In Fig. 1 we show the results of a Bayesian analysis of the orbit of HD 209458b. The solid curve is based solely on the radial velocity observations using the MCMC techniques described in this paper. The dotted curve is based on simulations in which the orbital period and phase have been fixed based on observations of the primary transits (Wittenmyer 2004; Laughlin et al. 2005). The dashed curve also incorporates the observation of the secondary eclipse observed in the infrared. To compute this last cumulative posterior distribution, we use MCMC to sample from the posterior distribution for orbital parameters based on the radial velocity and primary eclipse observations. We then treat this as the prior distribution for predicting the midtime of the secondary eclipse observed on December 6/7, 2004. We use a Gaussian likelihood with a standard deviation of 7 minutes and zero mean offset from the time predicted for a circular orbit (Deming et al. 2005). We then calculate the marginal posterior distribution for the eccentricity and integrate to obtain $p(e > e_o)$, the probability that the eccentricity of HD 209458b is at least e_o . Based on this posterior probability distribution, we find that $p(e > 0.008) = 0.32$, $p(e > 0.023) = 0.05$, and $p(e > 0.042) = 0.001$. Thus, it is unlikely that the current eccentricity of HD 209458b is sufficient to explain the unexpectedly large radius

of the planet.

6.2. HD 117207

Next, we consider the recently announced long period planet orbiting HD 117207. Radial velocity observations spanning 7 years were used to derive an orbital period of 7.2 ± 0.3 years and an eccentricity of 0.16 ± 0.05 (Marcy et al. 2005), where the error estimates were based on bootstrap-style resampling. The residuals to the best-fit orbit are consistent with a combination of measurement uncertainties (typically $\simeq 3\text{m s}^{-1}$) and the expected stellar jitter based on Ca II H & K emission, 3.6m s^{-1} . As noted by Marcy et al. (2005) the observations provide only modest constraints on the orbital parameters, since the orbital period is comparable to the duration of observations.

We use MCMC to perform a Bayesian analysis of the orbital parameters for this system, using the CTPDFs optimized for such systems from §4.13.2 (see Fig. 2). Our Bayesian analysis shows that the 68% credible interval for the marginalized posterior distribution includes periods in the range 7.3-11.7 years and eccentricities from 0.11 to 0.29. Thus, the uncertainties in the orbital parameters are significantly larger than suggested by bootstrap-style resampling. We note that even the constraints from our analysis may be optimistic, since we assume that there is only one planet in the system. If we also consider models which allow an additional planet, then the posterior distribution becomes even more broad.

6.3. *v* Andromedae

Many of the optimizations to the MCMC algorithm described in this paper have already been applied to the three planet system around *v* Andromedae (Ford et al. 2005). They used MCMC and several of CTPDFs from §4 to sample from the posterior probability distribution for orbital parameters assuming independent Keplerian orbits. That sample was used as the initial conditions for n-body integrations of the three planet system. N-body integration also demonstrated the robustness of these constraints to including the mutual planetary perturbations. Long-term direct n-body integrations were then used to place additional constraints on the orbital parameters, including the inclinations of the orbits to the plane of the sky and especially the relative inclinations between the orbits, by demanding dynamical stability. The resulting distribution for the dynamical state of the *v* Andromedae system provided strong evidence that the current eccentricities of planets c & d are the result of long-term mutual planetary interactions after planet d received an impulsive perturbation (most likely due to another unseen planet; Ford et al. 2005).

6.4. HD 37124

Radial velocity observations of the star HD 37124 have revealed three planets (Vogt et al. 2005). However, the discovery paper gave two sets of orbital solutions with very different properties for planet d: a preferred solution for planet d with an orbital period near 2200d, and an alternative solution with planet d in a ~ 30 d orbital period.

In principle, one could perform a Bayesian analysis of all three planets using MCMC simulations. In practice, this is not practical with the numerical techniques described in this paper. In particular, the CDPDFs used in this paper allow only local jumps based on the current state, and they are not appropriate for posterior PDFs which have multiple peaks separated by very deep and wide valleys. In the case of HD 37124, we are particularly interested in the relative probability of two orbital solutions with very different periods (~ 30 d and ~ 2200 d), so it is important to use a numerical technique which is capable of handling such strongly multi-modal posterior PDFs. One possibility is the technique of parallel tempering (e.g., Gregory 2005). Here we present an alternative method that is computationally more efficient and more robust for identifying small peaks in the posterior PDF. This is possible because the method described below assumes that the orbital parameters for the first two planets are not correlated with the orbital parameters of the third planet.

Since the orbits of two of the planets are well constrained by observations, we sample from the posterior distribution using a model that includes only the two previously discovered planets (b & c) modeled as on independent Keplerian orbits. We use this sample to calculate the posterior predictive distributions at the times of the actual observations and subtract the observed velocities to obtain the posterior predictive residual distribution at each time. We then analyze these velocity assuming they are due to a third planet (d), also assumed to be on an independent Keplerian orbit. We calculate the posterior distribution marginalized over all model parameters except period to estimate the significance of the detection of the third planet. This allows us to quantify the relative probabilities of these two solutions for the third planet. We find that $\gtrsim 99\%$ of the posterior probability distribution occurs near the orbital solution with an $P_d \sim 2200$ d.

While the above technique is very useful for searching for possible alternative orbital solutions for planet d, it could underestimate the uncertainty in model parameters if the orbital parameters for planets b & c are correlated with the orbital parameters for planet d. Therefore, after we identified a single plausible orbital period, we perform MCMC simulations using a three planet model to determine the posterior PDFs for the orbital parameters. Unfortunately, the discovery paper provided no estimates of the uncertainties in model parameters. Therefore, we present marginalized posterior probability distributions for the model parameter based on three planet MCMC simulations near the preferred solution (Fig. 3).

We have used this sample to calculate the posterior predictive distribution for the velocity as a function of time for several years into the future (Fig. 4). The width of the predictive distribution is presently $\simeq 5$ m s $^{-1}$, but increases to over 50m s $^{-1}$ within a year. This is not simply a result

of gradual loss of information with time, as the width of the predictive distribution increases and decreases significantly in a quasi-periodic manner. Radial velocity observations taken at the times when the predictive distribution has an unusually large width would be particularly valuable (Loredo 2003; Ford 2005b). It is important to note that the suggested times are not merely due to aliases when the star is behind the sun, below the horizon from Keck, or during new moon (when radial velocity planet surveys are unlikely to have telescope time), as the peaks in the width of the predictive distribution include times when HD 37124 is observable from Keck and during full moon. Therefore, there is no practical barrier that prevents measuring velocities near the times when the width of the posterior predictive distribution is maximized.

6.5. GJ 876

The multiple planet system around the M dwarf GJ 876 is particularly interesting, as there are two massive planets in a 2:1 mean motion resonance (Marcy et al. 2001). The mutual planetary perturbations are sufficiently strong that the orbits are precessing at $\sim 40^\circ/\text{yr}$ as shown in Paper I. Additional observations have been combined with direct n-body integrations to further constrain the allowed masses and orbital parameters and to detect a very low mass planet in a short period orbit (Rivera et al. 2005). Here we perform a Bayesian analysis of this system using a simplified model of precessing Keplerian orbits (Paper I). This model captures the most important aspects of the interaction between the outer two planets by adding a single free parameter ($\dot{\omega}_{bc}$, the precession rate of planets b & c), whereas a full dynamical model requires five additional free parameters (i and Ω for each of the three planets, minus one parameter which merely describes the rotation of the entire system). If we assume that the orbital planes are coplanar, then the physical system has one degree of freedom (the inclination of the orbital plane to the sky) which is not included in our model, and our model includes one parameter (the precession rate) which is really a function of the other model parameters. Therefore, in principle for each set of model parameters, we could determine the inclination at which the physical precession rate would equal the precession rate in the model. Unfortunately, the precession rate of the outer two planets is a non-linear function of multiple model parameters (inclinations and eccentricities) each of which have significant uncertainties, so that only loose constraints can be placed on each of i_b , Ω_b , i_c , and Ω_c . Therefore, we believe it makes sense to report the measurement of $\dot{\omega}_{bc}$, rather than several model parameters which are not yet well constrained.

We have used methods similar to those described in the previous section to analyze the HD 37124 system. Our analysis confirms the reality of a periodic signal with period, 1.9378d (see Fig. 5), as reported by Rivera et al. (2005). We also see smaller peaks near the periods of 0.66d, 2.05d, and 0.40d, but the posterior probability of all of these peaks sum to less than 0.1% of the primary peak. Note, that our analysis reveals no significant peak near the periods of 9, 13, or 120d, which were mentioned by River et al. (2005).

While our analysis is based on a simpler dynamical model than that of Rivera et al. (2005), our

method has several advantages. First, we use Bayesian rather than maximum likelihood methods, which allows us to make quantitative statements about the probability for secondary peaks. Second, our model captures the important planetary interaction by adding only a single free parameter, and yet our best-fit model provides a slightly smaller $\sqrt{\chi^2_{\nu}}$, χ^2 , and rms velocity scatter than any of the full n-body models reported in Rivera et al. (2005). This is because the overall precession of the outer two planets is well constrained by the observational data, but the data only weakly constrain the amplitude of the other mutual planetary perturbations. Additionally, our use of the posterior predictive residuals rather than the best-fit residuals provides a more robust tool when searching for additional periodicities. Finally, a secure detection of planet d with our simple model alleviates concerns that the periodicity might have been introduced by the dynamical modeling.

It should be cautioned that while our analysis demonstrates the reality of a 2.9d period in the velocity residuals (after subtracting the velocity perturbations by outer two planets), it does not necessarily imply that the signal is due to a planet. For example, in principle, a large moon around one of the outer two planets could also cause a periodic velocity perturbation. In the case of GJ 876, we have verified that the amplitude of the 2.9d signal is too large to be caused by a moon around either of the outer two planets. Nevertheless, as radial velocity searches detect periodicities with decreasing amplitudes, one should consider all possible causes for the detected velocity perturbations.

7. Conclusions

This and previous papers have demonstrated numerous advantages using Bayesian inference for analyzing the orbital parameters of extrasolar planets. Unfortunately, Bayesian analyses typically require calculating multidimensional integrals which can be computationally challenging. In Paper I, we introduced the method of MCMC, the Gibbs sampler, and the MH algorithm for performing these integrals. This made it practical to use MCMC to perform Bayesian analyses of the orbital parameters of several extrasolar planets. In this paper, we developed and tested several alternative CTPDFs to further improve the efficiency of MCMC. In particular, we recommend two sets of CTPDFs which together can accelerate the convergence of Markov chains by multiple orders of magnitude (see §4.13). These improvements make it practical to analyze all the known extrasolar planets and even multiple planet systems. We demonstrate our optimized MCMC algorithms by analyzing several actual extrasolar planet systems. We anticipate applying these algorithms to a large number of extrasolar planet systems to obtain more accurate orbital parameters and improve dynamical investigations of multiple planet systems.

Several significant challenges still prevent fully Bayesian analyses from being routinely applied to extrasolar planet observations. In particular, it can be quite computationally demanding to sample from the posterior distribution when the posterior distribution has several well separated modes. This commonly occurs for low-mass planets that are not yet clearly detected. It would be desirable to be able to analyze such planets, since the marginally detected planets can influence

the orbital parameters derived for other planets that have already been clearly detected around the same star. Another important challenge is developing computationally efficient means of performing Bayesian model selection, i.e., simultaneously considering models with zero, one, two, or more planets. This would allow planet detections to be based on Bayesian rather than maximum likelihood analyses. Gregory (2005a) has suggested parallel tempering as one possible approach, however even more efficient algorithms would be desirable.

We thank Floyd Bullard, Peter Driscoll, Debra Fischer, Greg Laughlin, Geoff Marcy, John Rice, Scott Tremaine, and an anonymous referee for valuable discussions. This research was supported in part by NASA grant NNG04H44g, and the Miller Institute for Basic Research. This research used computational facilities supported by NSF grant AST-0216105.

REFERENCES

- Benedict, G. F., et al. 2002, *ApJ*, 581, L115
- Bodenheimer, P., Laughlin, G., & Lin, D. N. C. 2003, *ApJ*, 592, 555
- Brown, T., Charbonneau, D., Gilliland, R., Noyes, R., & Burrows, A. 2001, *ApJ*, 552, 699
- Butler, R. P., Bedding, T. R., Kjeldsen, H., McCarthy, C., O’Toole, S. J., Tinney, C. G., Marcy, G. W., & Wright, J. T. 2004, *ApJ*, 600, L75
- Butler, R. P., et al. 1999, *ApJ*, 526, 916
- Butler, R. P., Marcy, G. W., Williams, E., McCarthy, C., Dosanjuh, P., & Vogt, S. S. 1996, *PASP*, 108, 500
- Cumming, A. 2004, *MNRAS*, 354, 1165
- Cumming, A., Marcy, G. W., Butler, R. P., & Vogt, S. S. 2003, *ASP Conf. Ser. 294: Scientific Frontiers in Research on Extrasolar Planets*, 294, 27
- Cumming, A., Marcy, G. W., & Butler, R. P. 1999, *ApJ*, 526, 890
- Deming, D., Seager, S., Richardson, L. J., & Harrington, J. 2005, *Nature*, 434, 740
- Driscoll, P. 2006, Master’s thesis, in preparation.
- Fischer, D. A., Marcy, G. W., Butler, R. P., Laughlin, G., & Vogt, S. S. 2002, *ApJ*, 564, 1028
- Ford, E. B. 2005a, *AJ*, 129, 1706
- Ford, E. B. 2005b, *AJ*, submitted

- Ford, E. B., Lystad, V., & Rasio, F. A. 2005, *Nature*, 434, 873
- Gelman, A., Carlin, J.B., Stern, H.S. & Rubin, D.B. 2003, *Bayesian Data Analysis*. New York: Chapman & Hall/CRC.
- Gilks, W. R., Richardson, S., & Spiegelhalter, D. J. 1996, *Markov chain Monte Carlo in practice* (Boca Raton, Fla.: Chapman & Hall)
- Gregory, P. C. 2005a, *ApJ*, 631, 1198.
- Gregory, P. C. 2005b, submitted, astro-ph/0509412.
- Kjeldsen, H., et al. 2003, *AJ*, 126, 1483
- Laughlin, G., Butler, R. P., Fischer, D. A., Marcy, G. W., Vogt, S. S., & Wolf, A. S. 2005, *ApJ*, 622, 1182
- Laughlin, G., Marcy, G. W., Vogt, S. S., Fischer, D. A., & Butler, R. P. 2005, *ApJ*, 629, L121
- Loredo, T. J. 2003. in *Bayesian Inference And Maximum Entropy Methods In Science And Engineering: 23rd International Workshop, Bayesian Adaptive Exploration*, AIP Conference Proceedings 707, eds. G. J. Erickson & Y. Zhai, 330
- Marcy, G. W., Butler, R. P., Fischer, D., Vogt, S. S., Lissauer, J. J., & Rivera, E. J. 2001, *ApJ*, 556, 296
- Marcy, G.W., Butler, R.P., Vogt, S.S., Fischer, D.A., Henry, G.W., Laughlin, G., Wright, J.T., Johnson, J.A. 2005, *ApJ*, 619, 570.
- McArthur, B. E., et al. 2004, *ApJ*, 614, L81
- Murray, C. D., & Dermott, S. F. 1999, *Solar system dynamics* (Cambridge, U.K. ; New York: Cambridge University Press)
- Pourbaix, D. 2002, *Astronomy and Astrophysics*
- Press, W. H., Teukolsky, S. A., Vetterling, W. T., & Flannery, B. P. 1992, *Numerical Recipes in C: the Art of Scientific Computing*. New York: Cambridge University Press.
- Rasio, F. A., & Ford, E. B. 1996, *Science*, 274, 954
- Marcy, G. W., Butler, R. P., Fischer, D., Vogt, S. S., Lissauer, J. J., & Rivera, E. J. 2001, *ApJ*, 556, 392
- Rivera, E., Lissauer, J., Butler, P., Marcy, G., Vogt, S., Fischer, D., Brown, T. & Laughlin, G. 2005, submitted to *ApJL*

Vogt, S. S., Butler, R. P., Marcy, G. W., Fischer, D. A., Henry, G. W., Laughlin, G., Wright, J. T.,
& Johnson, J. A. 2005, ApJ, 632, 638

Wittenmyer, R. 2004, Masters Thesis, San Diego State University

Wright, J. T. 2005, PASP, 117, 657

Table 1. Symbols Used in Multiple Sections

Symbol	Explanation
Indexes	
μ	indexes functions of model parameters
ν	indexes model parameters
i	indexes state in Markov chain
j_k	indexes observatory for k th observation
p	indexes planets
k	indexes observations
Variables	
$\vec{\beta}$	vector of scale parameters
χ^2	chi-squared statistic
ω	argument of periastron
Ω	longitude of ascending node
σ_k	effective uncertainty for k th observation
$\sigma_{k,\text{obs}}$	observational uncertainty in k th observation
σ_{\pm}^2	variance due to stellar jitter & unseen planets
τ	time of initial epoch
τ'	time of alternative epoch
$\vec{\theta}$	model parameters
$\vec{\theta}'$	model parameters for trial state
$\vec{\theta}_i$	model parameters for i th state of Markov chain
$\vec{\theta}_p$	set of model parameters for planet p
ν	degrees of freedom for Student's t -distribution
C_j	constant velocity offset for j th observatory
d_k	value of k th observation
$d_{k,\theta}$	prediction for k th observation with model, $\vec{\theta}$
e	orbital eccentricity
i	inclination of orbital planet relative to plane of sky
J	Jacobian of a transformation
K	velocity semi-amplitude
m	planet mass
m_{min}	minimum planet mass ($\sin i = 1$)
M_*	stellar mass
M	mean anomaly
M_o	mean anomaly at epoch $t = \tau$
M'_o	mean anomaly at epoch $t = \tau'$
\mathcal{M}	model description
P	orbital period
t_k	time of k th observation
T	true anomaly
T_{obs}	time span of observational data

Table 1—Continued

Symbol	Explanation
T_p	time of pericenter
$v_{*,\text{obs}}(t, j)$	observed radial velocity at time t & observatory j
Functions	
$p(\vec{d}, \vec{\theta} \mathcal{M})$	joint PDF for data & model parameters in model \mathcal{M}
$p(\vec{d} \vec{\theta}, \mathcal{M})$	likelihood assuming model \mathcal{M}
$p(\vec{\theta} \vec{d}, \mathcal{M})$	posterior PDF assuming model \mathcal{M}
$\widehat{R}(z)$	estimated Gelman-Rubin statistic for z
$\widehat{T}(z)$	estimated effective independent draws for z
$u_\mu(\vec{\theta})$	a function of model parameters

Table 2. Median $\log_{10} N_{Stop}$

T_{obs}/P	u_1^a	u_2^b	u_3^c	$(u_3, u_4, u_5)^d$
e = 0.01				
1	7.8	7.9	5.4	5.5
1.25	7.7	7.7	5.2	5.3
1.5	7.7	7.7	4.6	5.2
1.75	7.8	7.8	5.3	5.4
2	7.9	7.9	4.9	5.0
3	7.7	7.9	5.0	5.2
10	7.8	7.9	4.8	5.2
30	7.8	7.8	5.2	5.2
e = 0.1				
1	6.2	6.3	4.7	4.7
1.25	6.1	6.0	4.2	4.2
1.5	5.9	5.9	4.1	4.2
1.75	5.8	5.9	4.2	4.2
2	6.0	6.0	4.0	4.1
3	5.9	5.8	4.0	4.1
10	5.9	5.8	4.0	4.1
30	5.9	5.8	3.9	4.0
e = 0.5				
1	5.3	5.3	4.7	4.7
1.25	4.9	4.8	4.5	4.5
1.5	4.7	4.7	4.4	4.3
1.75	4.7	4.8	4.4	4.3
2	4.8	4.9	4.5	4.3
3	4.7	4.7	4.4	4.4
10	4.8	4.8	4.3	4.4
30	4.7	4.6	4.2	4.2
e = 0.8				
1	7.2	7.1	7.0	6.2
1.25	7.3	7.5	7.7	6.4
1.5	7.0	6.6	7.1	6.0
1.75	5.4	5.6	5.9	5.2
2	5.5	5.5	5.8	4.9
3	5.6	5.5	5.8	5.4

Table 2—Continued

T_{obs}/P	u_1^a	u_2^b	u_3^c	$(u_3, u_4, u_5)^d$
10	5.8	6.2	6.1	5.5
30	5.7	6.2	6.3	4.7

Note. — We list the median stopping time for Markov chains computed using four different sets of CTPDFs. The columns labeled u_1 and u_2 show stopping times using CTPDFs from Paper I. The columns labeled u_3 and (u_3, u_4, u_5) are based on the CTPDFs recommended in §4.13.

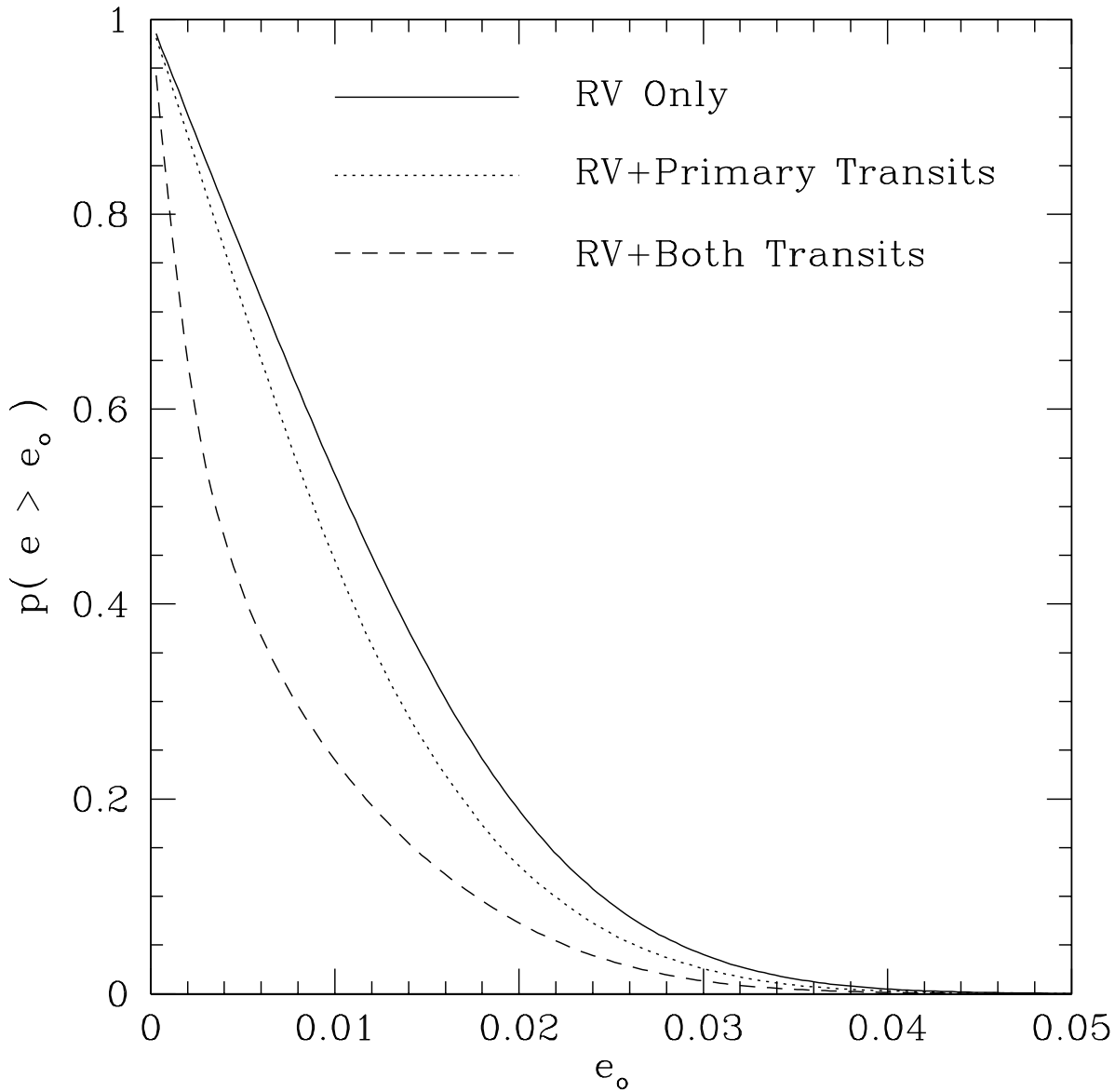


Fig. 1.— The posterior probability that the eccentricity of HD 209458b is greater than e_o . The solid curve is based on the radial velocity observations only. The dotted curve assumes a fixed orbital period and phase from the optical primary transit observations. The dashed curve also incorporates the time of the infrared secondary transit.

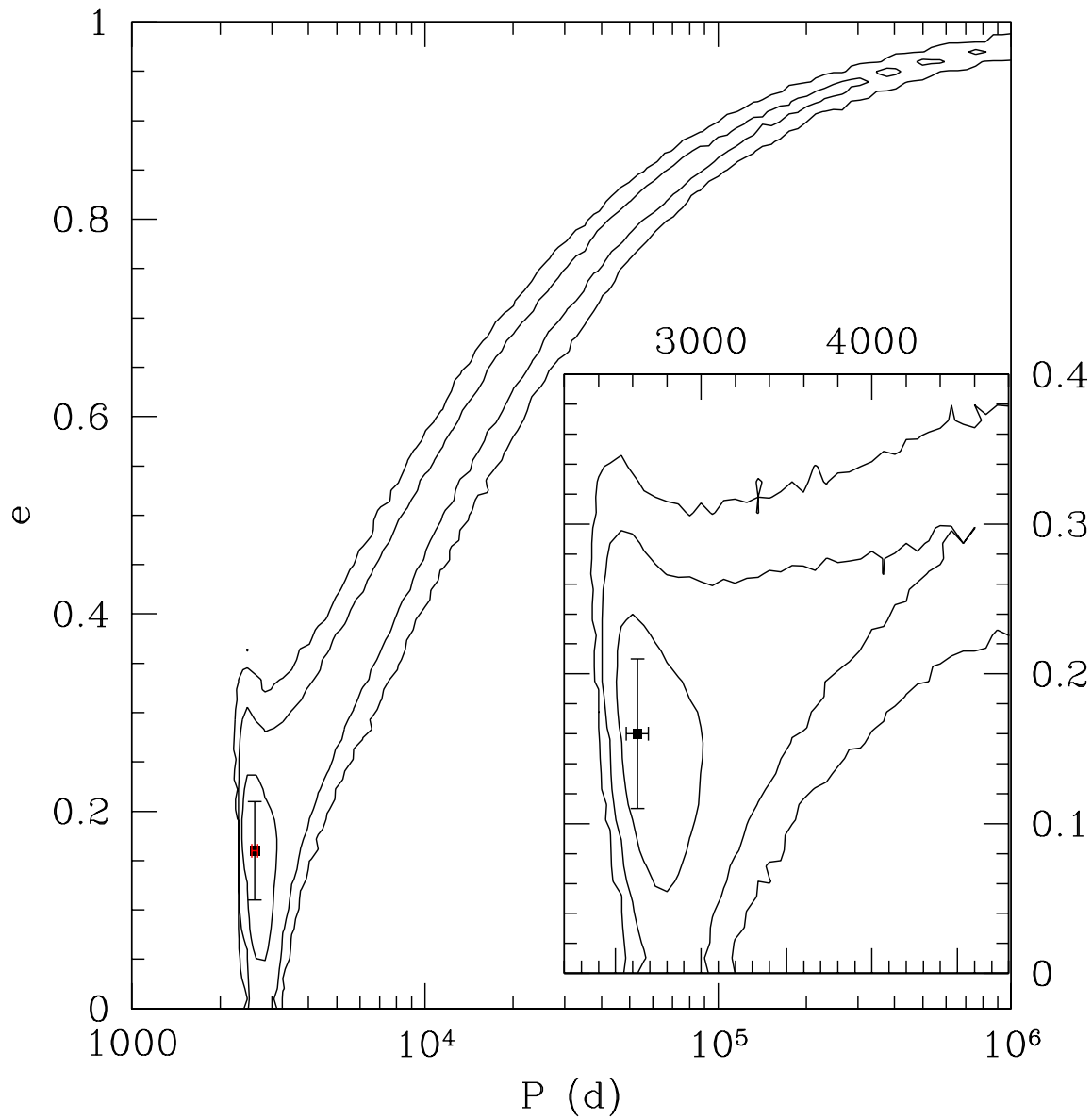


Fig. 2.— The marginalized posterior probability for the period and eccentricity of HD 117207b. The contours indicate 1, 2, and 3- σ credible intervals (defined to contain 68.3%, 95.4%, and 99.73% of the posterior probability distribution). The point and error bars show the published period, eccentricity, and error estimates (Marcy et al. 2005).

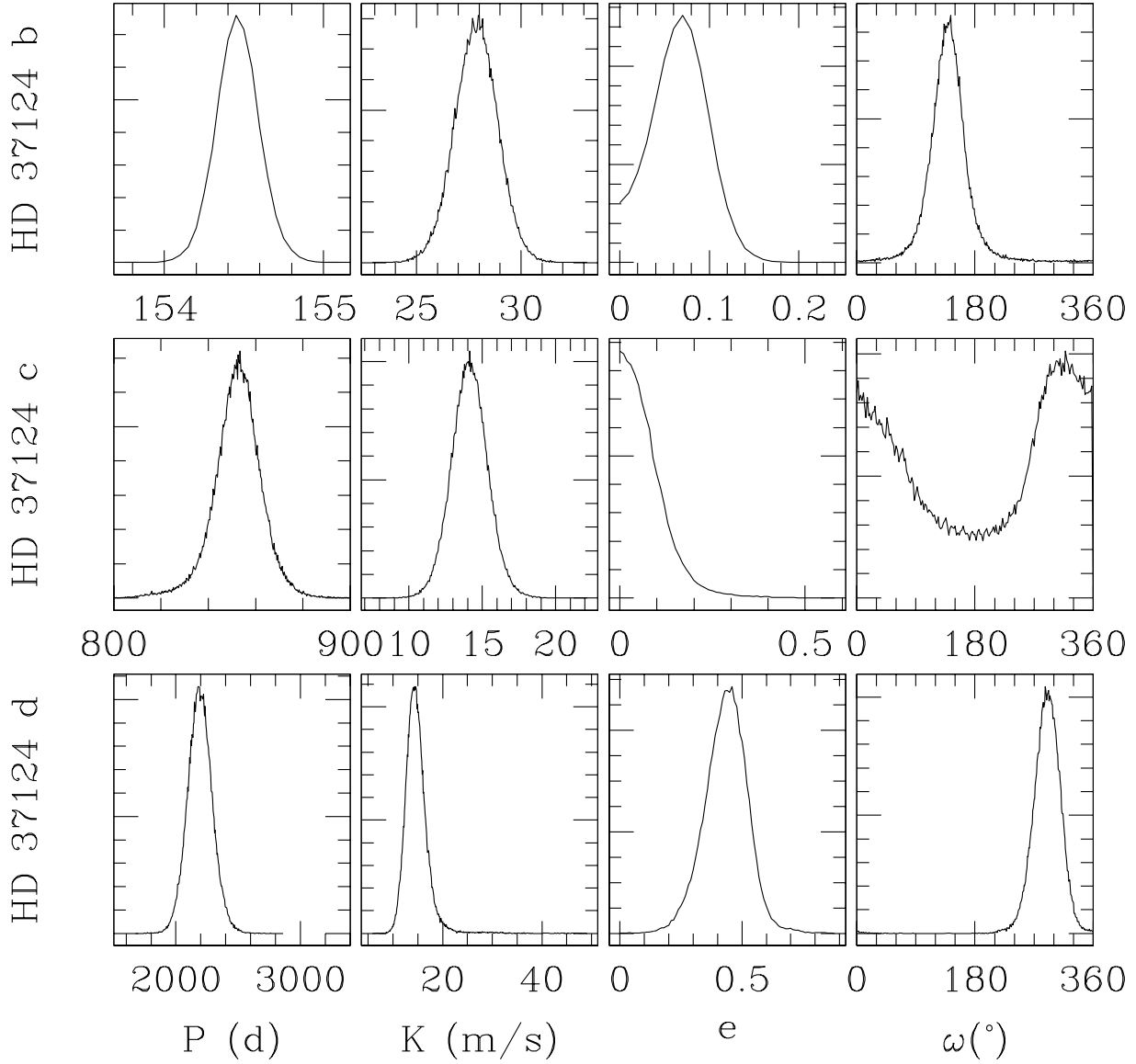


Fig. 3.— The marginalized posterior probability density for the orbital parameters of each of the three planets in the HD 37124 system. These distributions are based on a three planet model with no mutual interactions.

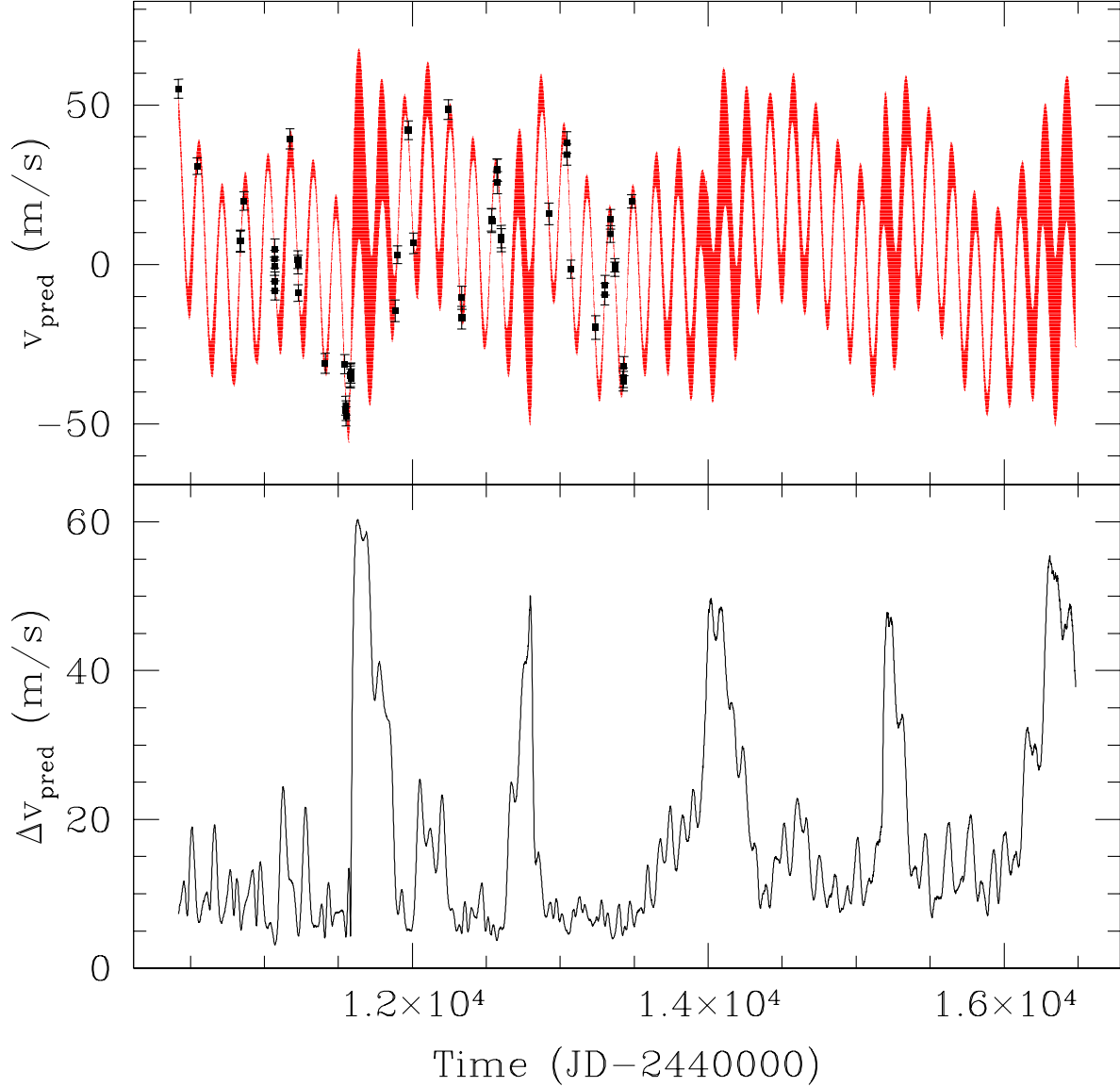


Fig. 4.— The shaded region in the top panel shows the 68% credible interval for the posterior predictive distribution for the velocity of HD 37124 as a function of time. We calculate the distribution of the predicted velocities from the posterior sample shown in Fig. 3. The points show the observational data and uncertainties. The lower panel shows the width of the 68% credible interval of the posterior predictive distribution as a function of time. The width is current $\simeq 5\text{m s}^{-1}$, but will increase to $\simeq 50\text{m s}^{-1}$ in the next year. Observations at these times will be particularly valuable for refining the orbit of this system.

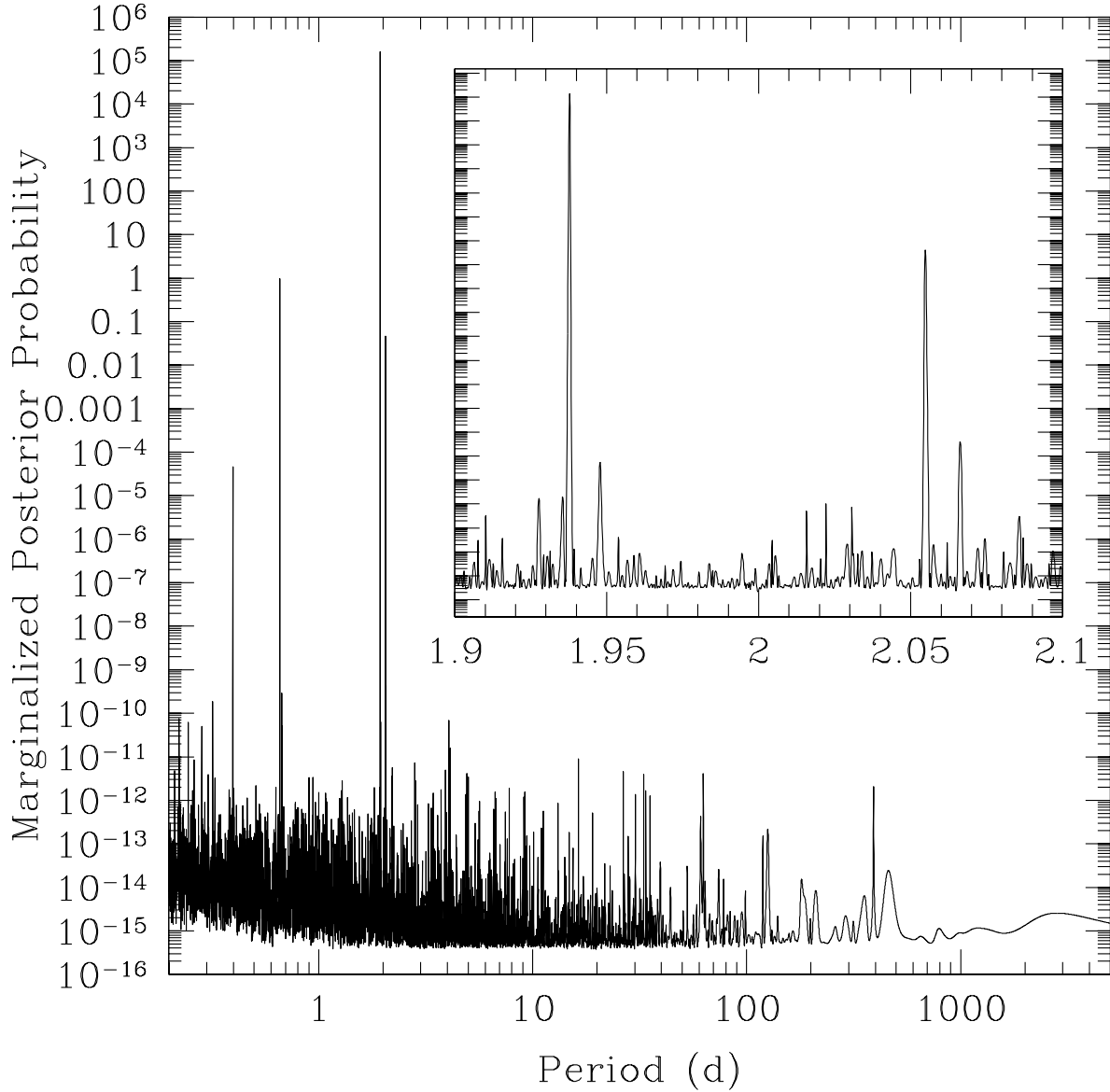


Fig. 5.— The marginalized posterior probability density as a function of the the orbital period of the low-mass planet GJ 876 d. First, we use MCMC to sample from the posterior probability distribution, assuming a model with only two planets on precessing Keplerian orbits. Then we calculate the posterior predictive residual velocity distributions. Finally, we calculate the posterior probability density for the orbital period of planet d, which we have assumed to be on a circular orbit. The inset zooms in on the periodicities near 2 days. Note that the largest peak contains over 99.9% of the posterior probability.